AD_____

Award Number: W81XWH-08-1-0386

TITLE: Genomic Analysis of Complex Microbial Communities in Wounds

PRINCIPAL INVESTIGATOR: Dr. Lance B. Price

CONTRACTING ORGANIZATION: Translational Genomics Reserach Institute
Phoenix, AZ 85004

REPORT DATE: January 2012

TYPE OF REPORT: Final Addendum

PREPARED FOR: U.S. Army Medical Research and Materiel Command
Fort Detrick, Maryland 21702-5012

REPORT DOCUMENTATION PAGE

Form Approved
OMB No. 0704-0188

1. REPORT DATE *(DD-MM-YYYY)*	2. REPORT TYPE	3. DATES COVERED *(From - To)*
01-01-2012	Final Addendum	2 JUN 2010 - 1JAN 2012

4. TITLE AND SUBTITLE
Genomic Analysis of Complex Microbial Communities in Wounds

5a. CONTRACT NUMBER

5b. GRANT NUMBER
W81XWH-08-1-0386

5c. PROGRAM ELEMENT NUMBER

6. AUTHOR(S)
Dr. Lance B. Price

E-Mail: lprice@tgen.org

5d. PROJECT NUMBER

5e. TASK NUMBER

5f. WORK UNIT NUMBER

7. PERFORMING ORGANIZATION NAME(S) AND ADDRESS(ES)
Translational Genomics Research Institute
Phoenix, AZ 85004

8. PERFORMING ORGANIZATION REPORT NUMBER

9. SPONSORING / MONITORING AGENCY NAME(S) AND ADDRESS(ES)
U.S. Army Medical Research and Materiel Command
Fort Detrick, Maryland 21702-5012

10. SPONSOR/MONITOR'S ACRONYM(S)

11. SPONSOR/MONITOR'S REPORT NUMBER(S)

12. DISTRIBUTION / AVAILABILITY STATEMENT
Approved for Public Release; Distribution Unlimited

13. SUPPLEMENTARY NOTES

14. ABSTRACT

The work that we conducted was aimed at moving wound research beyond the limitations of culture-based microbial analyses to enable comprehensive characterization of wound colonization and to fully evaluate its impact on healing. We successfully developed a novel, culture-independent approach for characterizing wound microbiota; we succeeded in applying statistical tools to begin characterizing the impact of antibiotic therapies and diabetes on wound microbiota; we used our novel strategies to define macro-scale spatial variation in chronic wound microbiota; we established research partnerships with MIHS to conduct prospective cohort studies on burn and chronic wounds; we enrolled a total of 71 patients into a prospective study of burn wound colonization and collected over 700 wound samples from these patients; we developed new protocols to isolate bacterial DNA from burn wounds with minimal exogenous DNA contamination; we developed a novel bioinformatics pipeline for identifying robust real time PCR targets for detection and quantification of clinical pathogens; and developed a comprehensive panel of TaqMan assays (n = 108) for detection of extraintestinal virulence factors in E. coli.

15. SUBJECT TERMS
Antibiotics, bacteria, community analysis, diabetes, pyrosequencing, wound, wound therapy, 16S rRNA gene

16. SECURITY CLASSIFICATION OF:			17. LIMITATION OF ABSTRACT	18. NUMBER OF PAGES	19a. NAME OF RESPONSIBLE PERSON
a. REPORT	b. ABSTRACT	c. THIS PAGE			USAMRMC
U	U	U	UU	48	19b. TELEPHONE NUMBER *(include area code)*

i. TABLE OF CONTENTS

Page

Table of Contents…… 03
Introduction ……..04
Body ……..05-45
Key Research Accomplishments…..……46
Reportable Outcomes……47
Conclusion……..48

I. INTRODUCTION

Relatively minor wounds, received in both war and peace, can become infected with bacterial pathogens, leading to substantial morbidity and mortality. To date, both culture-based and molecular-based studies have highlighted the remarkable diversity of bacterial pathogens in acute and non-healing wounds, but these diverse bacterial communities have yet to be fully characterized. An enhanced understanding of the complex wound microbial communities is crucial to the development of next-generation wound diagnostics and therapeutics. The purpose of this project was to develop and apply cutting-edge molecular technologies to characterize wound microbiota in a non-biased, culture-independent fashion.

II. BODY

FY07 Milestones

Milestone (original)		Comment
Clone 16S		see II.1.
Develop qPCR for bacterial DNA		see II.2.
Calculate Hum:Bact. DNA ratio		see II.3.
PhyloChip	**na**	Phylochip analysis was replaced by pyrosequencing analysis as described below. See II.4-II.6
Sequence clones		see II.1.
Characterize Phylotypes		see II.7.
Develop specific qPCR assays		see II.8.
Quantify major phylotypes (qPCR)		see II.9.
Spatial variation		see II.10.
Variation over time		see II.11.

FY08 Milestones

Milestone (original)		Comment
Establish sub-contract with MIHS		see II.12.
Complete IRB submissions		see II.13.
Purchase and place equipment		see II.14.
Develop database system		see II.15.
Collect and store burn wound samples		This objective was not achieved. see II.16.
Collect patient source samples		see II.17.
Collect metadata		see II.18.
Monthly shipments MIHS to TGen		see II.19.
Pyrosequence samples		see II.20.
Clone library analysis	**na**	see II.21.
Identify common phylotypes		see II.22.
Sequence genomic targets		see II.23.
Develop qPCR assays top 40		see II.24.
Validate qPCR assays		see II.24.

II.1. Clone 16S & Clone Sequencing

Prior to the pyrosequencing method, clone libraries were considered the gold standard for culture-independent, molecular characterization of bacterial communities. We used both methods to describe bacterial communities from chronic wounds. We found that both pyrosequencing and clone library analysis produced similar results, but pyrosequencing could provide much greater depth of analysis at a fraction of the cost.

16S rDNA-based clone library construction of wound samples. PCR primers were used to amplify the 16S rDNA from genomic DNA extracted from chronic wound samples provided by Johns Hopkins Wound Center. For clone library construction, primers AllBact_F1 (5′-CICCTACGGGIGGCWGCAG-3′, positions 338 to 357 of *E. coli*) and AllBact_R1 (5′-GGACTACCIGGGTATCTAATCCYITT-3′, positions 781 to 806 of *E. coli*) were used. All PCR thermocycling was carried out using Platinum *Taq* High-fidelity polymerase (Invitrogen Corp., Carlsbad, CA) in a DNAengine thermocycler (BioRad Laboratories, Hercules, CA). Each 50 µL PCR reaction contained: about 30 ng of purified genomic DNA, 200 µmol of each dNTP, 5.0 µL of 10x PCR Buffer, 3 mM Mg^{2+}, 450 nM of each primer, 1.0 U polymerase and 35.55 µL sterile 18 MΩ water. Amplification of 16S rDNA using the AllBact_F1/R1 primer set was achieved with a touch-down thermocycling program that consisted of a 1.5 min denaturation cycle at 95˚C followed by 33 cycles of 30 seconds at 95˚C, 30 seconds of annealing from 64˚C to 52˚C, stepping down 0.4˚C each cycle and 60 seconds at 72˚C, with a final elongation

cycle of 72˚C for 5 minutes. PCR products were purified using the AMPure SPRI-based PCR purification kit according to the manufacturer's recommendations (Agencourt Bioscience, Beverly, MA). Concentrations of purified products were determined by PicoGreen assay (Invitrogen) measuring fluorescence using an ND3300 Fluorometer (NanoDrop, Willmington, DE). Cloning and transformation of competent E. coli cells using PCR products from the AllBact_F1/R1 reactions was performed with the TOPO TA Cloning Kit for Sequencing (Invitrogen) according to the manufacturer's recommendations. The pCR 4-TOPO® vector was used in conjunction with TOP-10 chemically competent cells of *E. coli* (Invitrogen). After transformation, 200 µL of new S.O.C. media (Invitrogen) and the cells were incubated at 37˚C for one hour. Following incubation, 100 µL from each transformation was spread onto LB agar plates supplemented with 50 µg mL^{-1} kanamycin (Teknova, Hollister, CA). Plates were incubated overnight at 37˚C. Clone colonies were picked from the agar using sterile pipette tips. Picked clones were archived into individual wells of a 96-well microtiter plate containing 200 µL LB broth with a 7.5% concentration of glycerol (Teknova) and supplemented with 50 µg mL^{-1} kanamycin. After overnight incubation at 37°C with shaking, the archive plates were stored at -20°C

Plasmid preparation of clone libraries. Archived cell libraries were used to inoculate 384 well culture plates (Fisher Scientific) containing 200 µL of LB broth supplemented with 50 µg mL^{-1} kanamycin (Teknova). Each block was covered with breathable sealing tape and incubated for ~24 hours at 37°C with shaking at 400 rpm. Cells were pelleted by centrifugation at 4000 rpm for 10 min using an Eppendorf 5810R fitted with rotor model A-4-62. The supernatant was then removed by inversion of the blocks. 25 µL of GTE solution with RNAse A (100 µg mL^{-1}) was added and the cells were resuspended by vortexing. Fifty microliters of lysis solution 1 (0.2N NaOH, 1% SDS, made fresh from concentrated stock solutions) was added to each well. Wells were mixed by gentle shaking, then incubated at room temperature for 5 minutes. After incubation, 25 µL of 3M potassium acetate solution was added to each well followed by gentle shaking, then incubation for 5 minutes in a -20°C freezer. After freezer incubation, the plates were centrifuged for 20 minutes at 4,000 rpm. The supernatant from each well (75 µL) was transferred to a new 384 well microplate (Fisher) already holding 50 µL of cold isopropanol per well. The plates were incubated for 20 minutes in a -20°C freezer. Following incubation, the plates were centrifuged for 10 minutes at 4000 rpm. The supernatant was then decanted off and 75 uL of 70% ethanol was added to each well. The plates were centrifuged (10 minutes, 4000 rpm), the supernatant was poured off and the pellets were washed again. Following the second ethanol wash, the plates were allowed to air dry before the purified plasmid DNA was resuspended in 20 µL of filter sterilized 1X TE (pH 8.0, Fisher Scientific, Pittsburg, PA). Resuspended plasmid preparations were stored at -20°C until used for downstream applications.

Sanger sequencing and phylogenetic analysis of clone inserts. The 16S rDNA insert of fourty-eight plasmid preps from each wound library was amplified from the T7 promoter (5'-TAATACGACTCACTATAGGG-3') and T3 primer (5'-ATTAACCCTCACTAAAGGGA-3') sites on the TOPO-TA vector using recombinant *Taq* polymerase (Invitrogen) following the manufacturer's recommended concentrations and conditions. PCR products were stored at -20°C until further use. The following functions were performed by the TGen Sequencing Center (TGSC, Scottsdale, AZ). The T3/T7 PCR products were purified using solid phase reversible immobilization (SPRI)-based technology (AMPure®; Agencourt Biosciences Corp., Beverly, MA), resulting in the removal of unincorporated dNTPs, primers, and salts. PCR products were eluted in 30µl distilled H_2O. Both strands of each PCR product were sequenced as follows: Sequencing reactions were performed using 3µl (approximately 25ng) of purified PCR product in a 6µl reaction containing 0.33µl BigDye Terminator v3.1 premix, 3.2 pmol of T7 primer, and 1.03µl 5X BigDye sequencing buffer. Cycle-sequencing was performed for 35 cycles following the manufacturers recommendations on GeneAmp 9700 PCR machines (Applied Biosystems, Foster City, CA). Sequencing reactions were purified using CleanSEQ® (Agencourt Biosciences Corp., Beverly, MA) to remove unincorporated dye-terminators, and analyzed on 3730xl DNA analyzers (Applied Biosystems, Foster City, CA). Sequences from each wound library were analyzed using a PERL script we designed (RST v.1.4). The script searched each .seq file received from the TGSC for the AllBact_F1 and R1 sequence motifs and trimmed off any vector sequence as well as orienting all fragments so that the AllBact_F1 sequence is found at the 5′ end of each trimmed sequence. The script also filtered out any sequences that had ambiguous primer motifs, poor sequence quality and reads shorter than 400nt in length. Trimmed sequences from each library were aligned using the NAST alignment tool (DeSantis 2006. NAST) found on the GreenGenes database website (http://greengenes.lbl.gov). Each sequence was compared against their database with at most one non-redundant uncharacterized near neighbor reference and two non-redundant near neighbor references from isolate species retrieved for each sequence submitted. Query sequences were submitted in groups of 100 to 500 to minimize the number of redundant reference returns over

the whole library. NAST aligned sequences were imported into the phylogenetic database program ARB (Ludwig 2004), running on the Osiris server, which is a 64-Bit SMP machine with 4 dual-core AMD processors and 24 GB of memory running Redhat Enterprise and located at the Translational Genomics Research Institue High Performance Biocomputing Center (TGen HPBC, Phoenix, AZ). ARB was used to construct phylogenetic trees representing the 16S rDNA associations made by clones of each wound library to reference sequences retrieved from GreenGenes. This was achieved by first constructing a tree using only the reference sequences. The clone sequences were then imported and parsimoniously added to the reference tree by filtering out all but the region of the reference sequences where the cloned 16S fragments had aligned. Graphical and text enhancements of ARB trees were performed using Xfig v.3.2.4.

Rarefaction and abundance analysis. Sequences from each library were aligned as described above and used as the input for the Dnadist tool of PHYLIP 3.67 [Felsenstein, J. 1989] in order to generate distance matrices for each library. Rarefaction and Chao I richness estimations were determined by DOTUR [Schloss 2005] using the distance matrices from each library as input. The rarefaction and Chao I results were plotted using Microsoft Excel (Microsoft Corp., Redmond, WA). PHYLIP and DOTUR analysis was performed on the Osiris server mentioned above.

UniFrac analysis. Wound libraries were examined for β diversity associations using the program UniFrac (Lozupone 2005). These analyses were performed on a phylogenetic tree representing the associations between all of the clones without the presence of the nearest neighbor reference sequences. Clone operational taxanomic units (OTUs) were given environmental assignments according to the wound of origin. Using these environmental assignments, the tree was interrogated for meaningful associations between clone libraries. The 'clusterEnvironments' analysis was used to generate UPGMA clustering results. A tree representing the unweighted comparison of the different wounds was generated. This analysis takes into account the presence and absence of species between environments and groups the environments according to similarity of community structure. The resulting Newick formatted trees were visualized using NJplot and annotated using The Gimp 2.4. The UniFrac PCA analysis was used to generate principle component results from a comparison of the community differences between wounds. The unweighted analysis was performed using the default parameters. The principle components that explained the greatest amount of variation between environments were plotted.

Richness Estimations. In order to estimate sequence diversity in each sample, we generated rarefaction curves from our 16S rRNA gene clone libraries using three different cutoff levels for operational taxonomic units (OTUs): unique genus level (**Figure 1**). Rarefaction estimates indicated that we did not sample a sufficient number of clones to fully describe diversity at the unique sequence and species levels, but curves appear to be stabilizing for most samples at the genus level. Even as such, the diversity estimates generated using the 16S clone library sequences indicate a much greater level of microbial diversity than was measured by culture. The added depth provided by the Roche 454 platform will permit us to sample wound communities to a sufficient depth as to fully describe diversity at the species level.

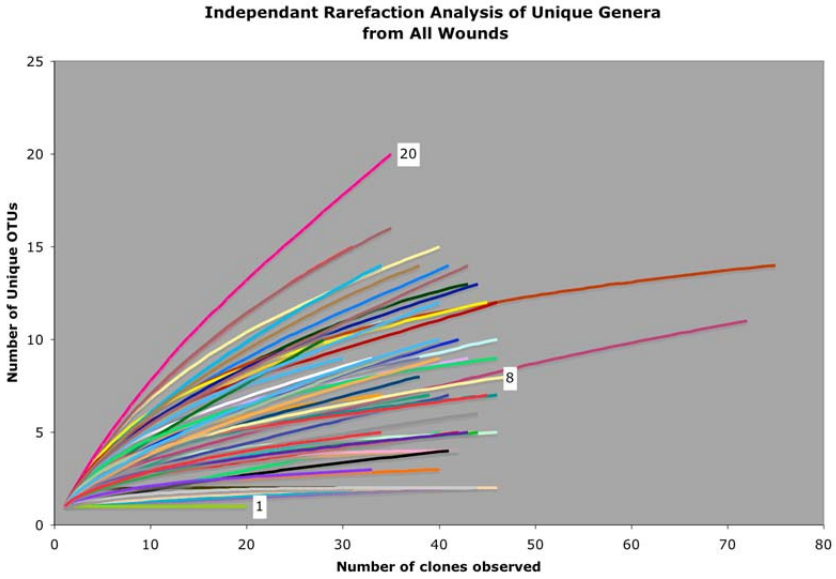

Figure 1. Rarefaction Analysis of Unique Genera from 16S clone libraries.

Wound Type Analysis. In order to test the hypothesis that different wound types have distinctive microflora, we performed three different analyses on our 16S rRNA gene clone library data. First, we used principle coordinate analysis to determine if wound type (neuropathic foot ulcer, venous stasis ulcer, decubitus ulcer, and other) could explain a significant portion of the community variation observed between the samples (**Figure 2**). This analysis revealed no significant association between wound types. Next, we divided observed species into oxygen tolerance groups (aerobic, anaerobic and facultative anaerobes; microaerophilic organisms were not observed) and then used the non-parametric Wilcoxon Rank-Sum (Mann-Whitney) test to compare ratios of oxygen tolerance groups between wound types in a pair-wise manner (**Table 1**). Ratios of oxygen tolerance types were not significantly different between the three wound types when compared to one another. These findings were supported using one-way ANOVA (data not shown). Finally, we compared the rate of colonization with group B Streptococcus between the different wound types using Chi^2 test to compare rate ratios, but again there were no statistically significant associations.

Diagnosis	**Proportion of Oxygen Types Mean (SD)**	**vs NFU (*p* value)**	**vs VSU (*p* value)**
Anaerobes			
NFU	0.159 (0.201)		
VSU	0.050 (0.098)	0.293	
DEC	0.312 (0.405)	0.473	0.160
Aerobes			
NFU	0.214 (0.293)		
VSU	0.516 (0.432)	0.119	
DEC	0.251 (0.171)	0.310	0.327
Facultative Anaerobes			
NFU	0.628 (0.266)		
VSU	0.437 (0.371)	0.206	
DEC	0.434 (0.385)	0.317	0.806

Table 1. Proportion Oxygen Tolerance Types, Pair-wise Comparison by Wilcoxon rank-sum test. NFU, neuropathic foot ulcer; VSU, venous stasis ulcer; DEC, decubitus ulcer.

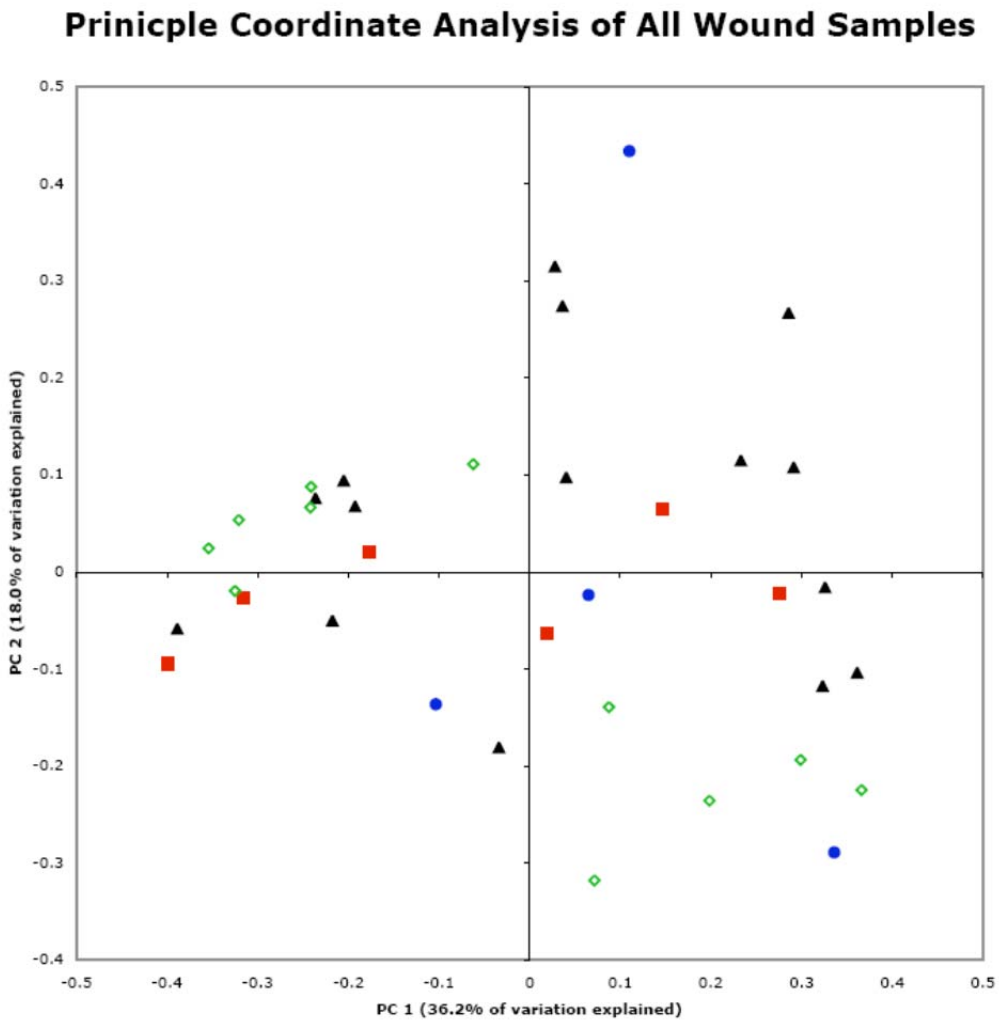

Figure 2. Principal Coordinate Analysis of Wound Type. Solid black triangles, neuropathic foot ulcer; Closed red squares, venous stasis ulcer; Closed blue circles, decubitus ulcer; Open green diamonds, other wound types.

Characteristic	Group B Strep*		Pair-wise Comparisons	
	Yes	No	NFU	VSU
NFU (n=15)	5	10		
VSU (n=5)	1	4	1.67 (0.251, 11.1); p = 0.573	
DEC (n=4)	0	4	Infinity; p = 0.179	0.0; p = 0.343

Table 2. Group B Streptococcus Positive Wound Types. NFU, neuropathic foot ulcer; VSU, venous stasis ulcer; DEC, decubitus ulcer.

II.2. Develop qPCR for bacterial DNA

We successfully developed a qPCR assay to accurately quantify bacterial DNA from mixed clinical samples. The 16S assay consisted of two primer pairs and a fluorescent probe. The selected primer and probe combination was, forward primer, 5'-TCCTACGGGAGGCAGCAGT-3' (Tm, 59 °C), the reverse primer, 5'-GGACTACCAGGGTATCTAATCCTGTT- 3' (Tm, 58 °C) and the probe, (6FAM)5'-TCAATCTGTCAATCCT-

3'(MGB) (Tm, 69°C). This primer set generated an amplicon 467bp (340-807bp in the E. coli K-12 16S rRNA gene). qPCR was performed on the Applied Biosystems 7900 platform using optical grade 96 and 384-well plates. The PCR reaction was performed in a total volume of 25µL in 96-well plates and a 10µL volume in 384-well plates using Invitrogen qPCR Supermix with UDG. The primer and probe concentrations were 900nM of the forward and reverse primers and the 250nM of the fluorogenic probe. The reaction conditions for DNA amplification were 50°C for 2 min, 95°C for 4 min and 40 cycles of 95°C for 15 s and 60°C for 1 min. Data analysis made use of Sequence Detection Software version 2.3 supplied by Applied Biosystems.

Validation. For both the *E. coli* K-12 genomic and plasmid standards, the detection range was between 200fg and 2ng of genomic DNA, in terms of copies this was between approximately 34 and 340,000 copies. The distribution of replicates was within 0.2 Ct's of the median, this deviation only increased as a result of pipetting error from either poor tip sealing or using a non-calibrated pipette. The average number of cycles between replicates was at 3.35 with an R^2 value greater than 0.998, indicating 100% PCR efficiency of the standard. Data from running the two standards side by side was used to calculate the copy number/cell ratio. *E. coli* K-12 genome weight was calculated as 4.8fg/genome. Using this information we calculated 8 copies per genome, consistent with the published copy number of 7 in the rrnDB.

Sensitivity of the assay in detecting *Escherichia coli* rDNA. Taqman® assays allow determination of the PCR cycle at which the increase in fluorescence of the reporter dye reaches a threshold cycle (Ct). A Ct value is indicative of the log of the amount of target DNA, which is directly attributable to the log of the number of bacteria in the sample (adjusted to the number of gene copies per genome). The *Escherichia coli* standard had seven copies of rDNA in each copy of the chromosome, and had a mass of approximately 5fg. Using *Escherichia coli* as a standard, we consistently detected between 200 fg or 40 *Escherichia coli* cells and 2ng *Escherichia coli* DNA or approximately $4x10^5$ *Escherichia coli* cells. Although measurements outside of this range are possible, chances increase for a two-fold or more error in estimation. The greatest barrier to achieving greater assay sensitivity on the low end of the spectrum was contaminating bacterial DNA in commercially supplied reagents. The degree varied between different lots of the Invitrogen Supermix UDG, illustrating the importance of running several negative controls with each assay in order to determine the lower bound. The most likely explanation for this contamination is trace amount of DNA that makes it into reagents during polymerase preparation. We confirmed this contamination when observing rDNA in reagent mixes and negative controls containing no added bacterial DNA. To minimize this problem we attempted to use Environmental Master Mix from Applied Biosystems (which has been purified of all genomic DNA) however results from these runs yielded lower sensitivity that with regular master mix. We also attempted treating the Invitrogen Supermix with DNAse I (Invitrogen), then inactivating the enzyme by heating to 85°C for 15 minutes. Although this did remove late DNA amplification in the negative controls, it also degraded amplification efficiency in regular samples and had no improvement in assay sensitivity.

Detection and quantification of panel DNAs. We determined that the universal assay did not amplify human DNA (obtained from Applied Biosystems), plant DNA (from a Pinyon Pine tree), or fungal DNA (representatives of four fungal divisions were tested). This broad panel also allowed us to determine that variations in rDNA copy number had no direct correlation to differences copy between standardized samples when using this assay. When tested against the 21 panel organisms, the assay reliably amplified all members of the panel. Once standardized, 17 of the 21 members of the panel amplified within 1.5-2 Ct's of the standard, resulting in a quantity difference of 40%. *Borrelia burgdorferii* and *Coxiella burnetii* amplified an average of four cycles later than the *E. coli* standard, indicating an underestimation of genomic quantity by 100-150%. *Mycobacterium pneumoniae* and *Anabaena variabilis* consistently amplified 9 Ct's from the standard, underestimating the actual genomic quantity by 1000-fold. PCR efficiency was initially checked for each DNA by multiplexing the 16S assay with the Exogenous IPC from Applied Biosystems. Doing this decreased sensitivity and only worked well with Applied Biosystems Taqman® Master Mix. To overcome this problem we opted to run the IPC independently and verify results by creating five serial ten-fold dilutions of each isolate and checking for 100% PCR efficiency along these dilutions.

All isolates exhibited no inhibition with the IPC assay. In addition all isolates except for *Borrelia burgdorferii*, *Coxiella burnetii*, *Mycobacterium pneumoniae,* and *Anabaena variabilis* had 100% +/- 10% PCR efficiency among serial dilutions. Although no inhibition was detected when using the IPC, *C. burnetii* and *B. burgdorfeii* amplified with approximately 3.5, 3.7, and 4 cycle differences between serial dilutions from 2ng to 2pg of genomic DNA, and had an average efficiency of only 85%. *Mycobacterium pneumoniae,* and *Anabaena variabilis* similarly had no detectable inhibition when checked with the IPC, however performing a serial dilution

down from 2ng of DNA resulted in >4 Ct difference, both isolates amplified the 200pg quantity at the trace DNA threshold of cycle 34.

We also tested for amplification anomalies as a result of complex mixtures composed of multiple organisms, we ran groups of DNAs in a mixture of 2, 4, 6, and 8 standardized genomic DNA extracts from different bacteria. These runs yielded results that were directly proportional to the sum of the concentrations of individual DNAs (data not shown). However, when mixtures of larger numbers of DNAs were attempted, the total DNA concentration exceeded 1ng/µL and the intervals between serial dilutions of these mixtures decreased. The logarithmic relationship was restored by diluting individual DNAs and re-pooling into groups of 10 and 12 organisms. More complex mixtures were not attempted because at extremely low dilutions there was no qPCR-independent method of verifying individual DNA concentrations added to the total mixture.

The *E. coli* genomic DNA standard was mixed with 1%, 10%, 50%, 90%, and 99% *Saccharomyces cereviciae* DNA then with again with the same ratios of human DNA. There was slight inhibition of the standard at the 99% non-target concentration of both human and *S. cerevisiae* DNAs. This experiment was repeated with the mixtures of 4 panel DNAs and yielded the same results. Following these experiments the assay was tested with an additional panel of 30 pathogens that commonly cause Community Acquired Pneumonia/SEPSIS. All organisms in that group amplified within 1.5 – 2 Ct's of the standard and were accurately quantified based on earlier measurements of genomic DNA quantity.

II.3. Calculate Human:Bactial DNA ratio

Bacterial load is considered a critical aspect of wound healing. Traditionally, bacterial load is calculated by weighing, homogenizing and culturing wound biopsy tissues. Load is then reported per mg of tissue. This method is not conducive to calculating bacterial load based on swab samples and relies on the accuracy of balances that are typically not calibrated to weigh tissue samples on the mg scale. In order to develop a more accurate and repeatable method for measuring bacterial load from both tissue and swab samples, we developed a method whereby bacterial load can be estimated based on the ratio of bacterial DNA to human DNA. Bacterial DNA is measured using our custom, in-house qPCR assay for the 16S gene (described in quarter 1 report) and human DNA is measured using a qPCR assay for the human *Alu* gene. The 16S gene copy number can be used to determine the approximate number of bacteria in a sample. Likewise, the *Alu* gene copy number can be used to estimate the number of human cells in a sample. Finally, bacterial load is calculated by dividing the number of bacterial cells to the number of human cells.

Bacterial to Human Cell Ratio: calculation methods. The wound samples were extracted using the protocol "Isolation of Bacterial Genomic DNA from Clinical or Environmental Samples" (version 1.4). Once extracted, the samples were amplified using ABI Internal Positive Control (IPC) kit to detect the presence of PCR inhibitors. No inhibitors were detected. The bacterial load was quantified by real time-PCR using 16S target specific primers and prope (developed in quarters 1 and 2) against dilutions (neat to 1:100 dilution). A plasmid standard curve with 10-fold dilution was added to each plate (10^8 to 10^2 copies of 16S gene). The number of copies of the 16S gene was calculated based on the standard curve and the neat values were back-calculated including the respective dilution factor. The number of bacterial genomes was calculated by dividing the copy number by 4.13 (the average number of 16S genes in an individual bacterium).

The human cell load was quantified using the *Alu* Human Target qPCR Assay. This assay targets the human *Alu* subfamily Ya-5 gene using the primers Forward: GACCATCCCGGCTAAAACG, Reverse: CGGGTTCACGCCATTCTC and probe 6FAM-CCCCGTCTCTACTAAA-MGBNFQ on the LightCycler® 480 Real Time PCR Instrument (Roche). The samples were tested with dilutions (neat to 1:100 dilution) and were run along side a plasmid standard curve of 10-fold dilutions (10^8 to 10^2 copies of the *Alu* gene). To calculate the human cell load for each sample the quantity from the qPCR results was multiplied by the dilution factor to generate the calculated or expected copy number in a neat sample, this calculated neat copy number was then divided by 5000 (the number of copies of the *Alu* subfamily Ya-5 gene found in a diploid human genome or cell).

The ratio of bacterial to human cells was also calculated for each sample by dividing the number of bacterial genomes by the number of human genomes.

Results. We used the qPCR method described above to calculate the bacterial load in 32 chronic wound samples. Bacterial loads ranged from 0.03 to 5184 (average, 191) bacteria per human cells. Fourteen of the wound samples were from patients who had received antibiotics within the past two weeks. We stratified samples by recent exposure to antibiotics and compared bacterial load using a Mood's median test (The data were not normally distributed; therefore, s Mood's median test was run on the data). There was a significant

difference in the median bacterial load for patients who took antibiotics versus patients who did not take antibiotics (*p*-value = 0.033) (**figure 3**).

Conclusions. The qPCR-based bacterial load assay that we have developed is a rapid, culture-independent method for calculating bacterial load in wounds. This method can be used for a wide array of clinical samples including swab, curette and biopsy samples from acute and chronic wounds. Using the ratio of bacterial to human DNA frees the clinical researcher from having to estimate tissue weights or swabbed surface area for bacterial load calculations. Here we have applied it to chronic wound samples and detected a significant reduction in bacterial load associated with recent antibiotic exposure.

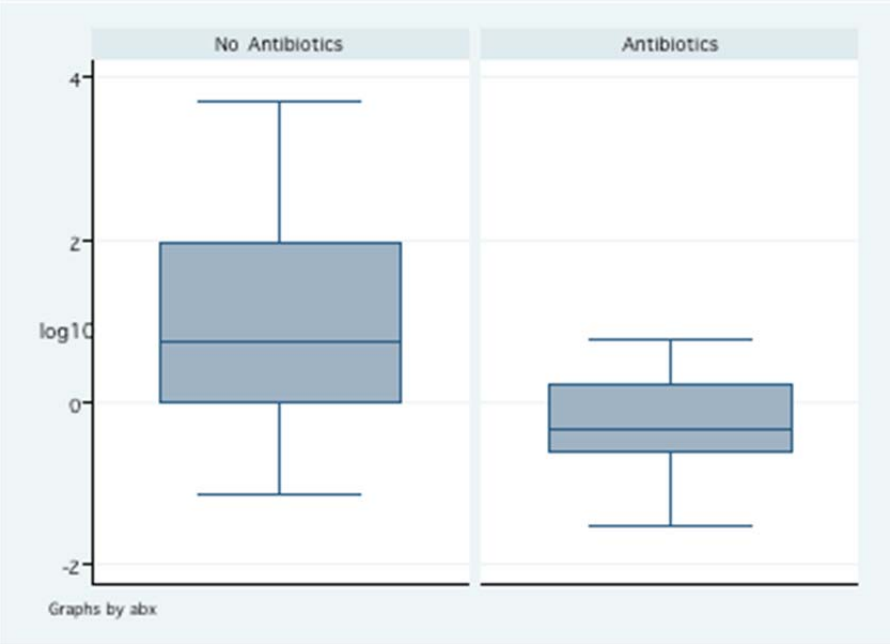

Figure 3. Box plot of $\log_{10}$ transformed bacterial load data from patients with and without recent exposure to antibiotics.

II.4. PhyloChip Analysis

We (and other groups) have found that pyrosequencing is a much more cost-effective and reliable way to characterize complex bacterial communities from wounds and other sample types and thus redirected our efforts originally planned for PhyloChip analyses to developing the pyrosequencing pipeline described herein.

II.5. Develop Pyrosequence Data Analysis Pipeline (replacement for PhyloChip)

Recent advances in pyrosequencing technology provide the potential to characterize complex bacterial communities in a culture-independent fashion at depths not possible previously. One of the greatest challenges to utilizing this platform is having the bioinformatic and statistical capabilities necessary to make use of the hundreds of thousands of DNA sequences that are created in each run. Over the past year, we have developed a data analysis pipeline for handling 16S rRNA gene sequences from the Roche FLX454 pyrosequencer. The methods described below will be published in a manuscript later this month (appendix B).

Experimental sequences were processed using a custom PERL script, which performs the following: the script filtered the sequence files and retained only sequences that were 200-nt or longer. It then searched for a single barcode sequence in each FASTA sequence, binned each sequence accordingly, and scanned each binned sequence for the 16S forward primer sequence. The script then trimmed off the forward primer sequence and oriented the remaining sequence such that all sequences begin with the 5' end according to standard sense strand conventions. As a result of our processing, sequences that were shorter than 200-nt or had multiple barcode or primer motifs were excluded from the analysis. We included only sequences with the forward primer motif to ensure that the highly informative V3 region was available for taxonomic assignment. The trimmed sequences from each barcode bin were aligned using the NAST alignment tool (http://greengenes.lbl.gov) [DeSantis 2006]. After alignment, the number of sequences examined per wound sample was equilibrized to 300 sequences by sampling randomly without replacement to facilitate subsequent taxa abundance analyses. Samples with fewer than 300 sequences were excluded. The cutoff of n = 300 was

established based on richness (rarefaction) and diversity (Shannon-Weaver Index) analyses using DOTUR [Schloss 2005], which indicated that samples were sufficiently sampled after ≥300 sequences.

Taxonomic assignment. Unaligned, sequences in the equilibrated dataset were given taxonomic assignments at a bootstrap confidence range of ≥95% using the Ribosomal Database Project's Naïve Bayesian Classifier tool (RDP classifier) [Wang 2007; Cole 2009].

Rarefaction and diversity analyses. Distance matrices based on taxa abundance were generated with the Dnadist tool of PHYLIP 3.67 using the default settings [Felsenstein 1989]. Rarefaction and Shannon Weaver index estimations were determined by DOTUR [Schloss 2005] and plotted in Microsoft Excel (Microsoft Corp., USA).

Statistical analyses. All statistical analyses were performed using our equilibrated dataset (n = 300 sequences per sample). Community-scale multivariate analyses including non-metric multidimensional scaling (nMDS), multiresponse permutation procedure (MRPP), and the Dufrêne & Legendre indicator analyses were performed in R [R Development Core Team 2008] using statistical packages vegan [Oksanen 2009], ecodist [Goslee 2007], BiodiversityR [Kindt 2005], and labdsv [Roberts 2007]. The nMDS analysis is a nonparametric ordination-based method for reducing ecological community data complexity and identifying meaningful relationships amongst communities, while the MRPP analysis is another nonparametric method for testing the null hypothesis of no-difference between communities by comparing the experimental with the expected within-group difference through an iterative randomization process. The indicator species analysis further identifies the bacterial taxa that are significantly unique to each environment (e.g., clinical variables of interest). The nonparametric nature of these ecological analysis methods is highly suitable for human bacterial community data, which are frequently zero-rich, highly-skewed, and non-normal and remains non-normally distributed post-data transformation. Significance level for MRPP and the Dufrêne & Legendre indicator analyses were set at $\alpha = 0.05$.

Comparative analysis of mean indicator prevlaence between environments (e.g. diabetics versus non-diabetics) were also performed in R using custom codes. Briefly, using the taxa abundance-based distance matrices, a t-statistic was calculated and the underlying null distribution was estimated using Monte-Carlo based resampling (n = 10,000 permutations). A two-tailed empirical p-value was generated by comparing the unpermuted data with the estimated null distribution. Significance levels were set at $\alpha = 0.05$ with the appropriate Bonferroni correction (α/n), with n = number of tests performed for a single environment.

Assessment for the interaction between antibiotic use and diabetes and the percent agreements in the comparison of 16S rRNA gene-based and culture-based results were performed using multivariate logistic regression and the kappa-statistic, respectively in STATA 9 (StataCorp, USA).

II.6. Pyrosequence bacterial communities from wound samples

In addition to developing the pyrosequencing analysis pipeline described above, we have also developed a highly efficient method for analyzing complex bacterial communities using the 16S rRNA gene sequence. The methods described below will be published in a manuscript later this month (appendix B).

Pyrosequencing library synthesis for parallel tagged sequencing on the 454® platform. The 16S rRNA gene was amplified in two replicate 50 µl reaction volumes. In each 50 µl reaction, 3 µl was added to 47 µl of PCR reaction mix containing 450 nM of each broad range forward (5'-CCTACGGGAGGCAGCAGT-3') and reverse primer (5'-GGACTACCAGGGTATCTAATCCTGTT-3') [Nadkarni 2002], 1X PCR buffer without $MgCl_2$ (Invitrogen), 3 mM $MgCl_2$, 0.2 mM dNTP mix, 0.02 U platinum *Taq* (Invitrogen) using the following touch-down PCR condition: 90s at 95°C for initial denaturation, 30s at 95°C for denaturation, 30s at 64°C for annealing, 30s at 72°C for extension with the annealing temperature decreasing by 0.3°C for each subsequent cycle for 34 cycles, followed by 5 min at 72°C for final extension. Subsequent purification, blunt-end repair, adapter ligation, amplicon quantification and pooling, restriction digestion, and pyrosequencing library generation were carried according to a previously published protocol [Meyer 2008]. The sample-specific, palindromic, self-hybridizing barcodes used in the tagging reactions were generated using a self-complementary 8-nt barcode and a rare restriction site according the same protocol.

Pyrosequencing using the 454® platform. The pooled tagged single-stranded pyrosequencing library underwent fusion PCR and pyrosequencing using a Roche 454 FLX Pyrosequencer (Roche Life Sciences, USA) according to the manufacturer instructions [McKenna 2008] at the Institute for Genome Sciences, Genomic Resource Center.

II.7. Characterized Phylotypes among Wounds

We used 16S clone libraries, 16S PhyloChips and two different 16S pyrosequencing methods to characterize phylotypes in this study. Of these methods, we found that pyrosequencing was the most cost effective method for characterizing complex microbial communities in wounds. Using pyrosequencing and the RDP Naïve Bayesian Classifier, we characterized the genus level phylotypes from 74 chronic wound samples collected at the Johns Hopkins Wound Center; however, only 66% of the sequences could be named to the genus level with high confidence (>95% confidence). Despite this limitation, 99 unique bacterial genera were identified among the samples (**Table 3**). *Staphylococcus* was the most common genera identified among samples (**Figure 4**). Other genera including *Streptococcus, Paracoccus, Corynebacterium and Ralstonia* were also found in relatively high concentration among samples included (**Table 3**; **Figure 4**). Most notably missing from the genera identified in the wounds were those belonging to the family Pseudomonadaceae—the second most common bacterial family found in chronic wounds (**Table 4**; **Figure 5**). This discrepancy highlights the limitations of the current 16S databases and classifiers to name genera belonging to certain bacterial families including Enterobacteriaceae and Pseudomonadaceae. Given the clinical importance of these genera, this is a limitation that must be addressed. Until this shortcoming is remedied, we have chosen to conduct all of our wound analyses on family-level phylotype data. We successfully named 98% of the sequences to family-level phylotypes with high confidence (>95%) and identified 76 unique families among the 74 wound samples (**Table 4**; **Figure 5**). These results further underscore the complexity of chronic wound microbiota. Likewise, these results also highlight the importance of developing rapid, culture independent detection methods which is the goal of our future work.

Table 3. Ninety-nine genus-level phylotypes identified among the 74 chronic wound samples collected at the Johns Hopkins Wound Center. Phylotypes are listed in order of prevalence (most to least prevalent).

Genus	No. Wound samples positive	Ave. copy number per positive	Total no. sequences (39,220 total)
Staphylococcus	65	178	11539
Streptococcus	30	87	2603
Paracoccus	12	216	2596
Corynebacterium	46	40	1817
Ralstonia	62	18	1088
Anaerococcus	30	30	894
Sanguibacter	7	96	675
Carnobacterium	6	110	657
Finegoldia	24	17	413
Peptoniphilus	20	18	358
Porphyromonas	7	49	340
Chryseobacterium	6	51	306
Bacteroides	8	25	196
Prevotella	12	15	185
Rhizobium	5	35	174
Peptostreptococcus	5	33	163
Bacillus d	7	20	142
Gemella	7	19	135
Enterococcus	9	13	120
Parvimonas	8	14	110
Roseomonas	3	37	110
Alcaligenes	6	17	101
Acidaminococcus	3	32	97
Burkholderia	26	3	83
Fusobacterium	5	15	75
Peptococcus	5	14	71
Bartonella	5	13	65
Gardnerella	5	12	60

Desemzia	3	18	55
Sphingomonas	28	2	55
Aerococcus	7	8	53
Actinomyces	13	4	48
Fastidiosipila	6	8	48
Streptomyces	8	5	42
Dialister	8	5	38
Helcococcus	9	4	34
Bacillus c	6	5	30
Lachnospiraceae Incertae Sedis	5	6	30
Actinobaculum	4	7	27
Achromobacter	16	1	22
Arcanobacterium	8	3	21
Rothia	4	5	21
Erysipelotrichaceae Incertae Sedis	2	11	21
Veillonella	7	3	18
Arthrobacter	7	2	16
Propionibacterium	11	1	15
Atopobium	3	5	14
Brevibacterium	5	3	13
Phyllobacterium	8	2	13
Wolbachia	2	7	13
Granulicatella	3	4	12
Methylobacterium	9	1	12
Cloacibacterium	7	1	10
Dermabacter	3	3	9
Megasphaera	3	3	9
Brochothrix	1	8	8
Bulleidia	3	3	8
Cupriavidus	5	1	7
Peptostreptococcaceae Incertae Sedis	1	7	7
Lactococcus	4	2	7
Paenibacillus	1	5	5
Clostridium	1	5	5
Globicatella	2	3	5
Mobiluncus	1	4	4
Cellulomonas	2	2	4
Roseiflexus	1	4	4
Eggerthella	3	1	4
Lactobacillus	3	1	4
Bradyrhizobium	2	2	4
Acidobacteriaceae Gp16	1	3	3
Microbacterium	3	1	3
Nocardioides	3	1	3
Bacillus a	3	1	3
Mesorhizobium	2	2	3
Micrococcus	2	1	2
Macrococcus	2	1	2
Phenylobacterium	2	1	2
Oribacterium	2	1	2
Deinococcus	2	1	2
Pediococcus	1	2	2

Pedobacter	2	1	2
Acidobacteriaceae Gp7	1	1	1
Blastococcus	1	1	1
Kineococcus	1	1	1
Leucobacter	1	1	1
Quadrisphaera	1	1	1
Williamsia	1	1	1
Pasteuriaceae Incertae Sedis	1	1	1
Jeotgalicoccus	1	1	1
Bifidobacterium	1	1	1
Bordetella	1	1	1
Oligella	1	1	1
Caulobacter	1	1	1
Turicibacter	1	1	1
Flavobacterium	1	1	1
Isosphaera	1	1	1
Rubrobacter	1	1	1
Dyadobacter	1	1	1
Thermus	1	1	1

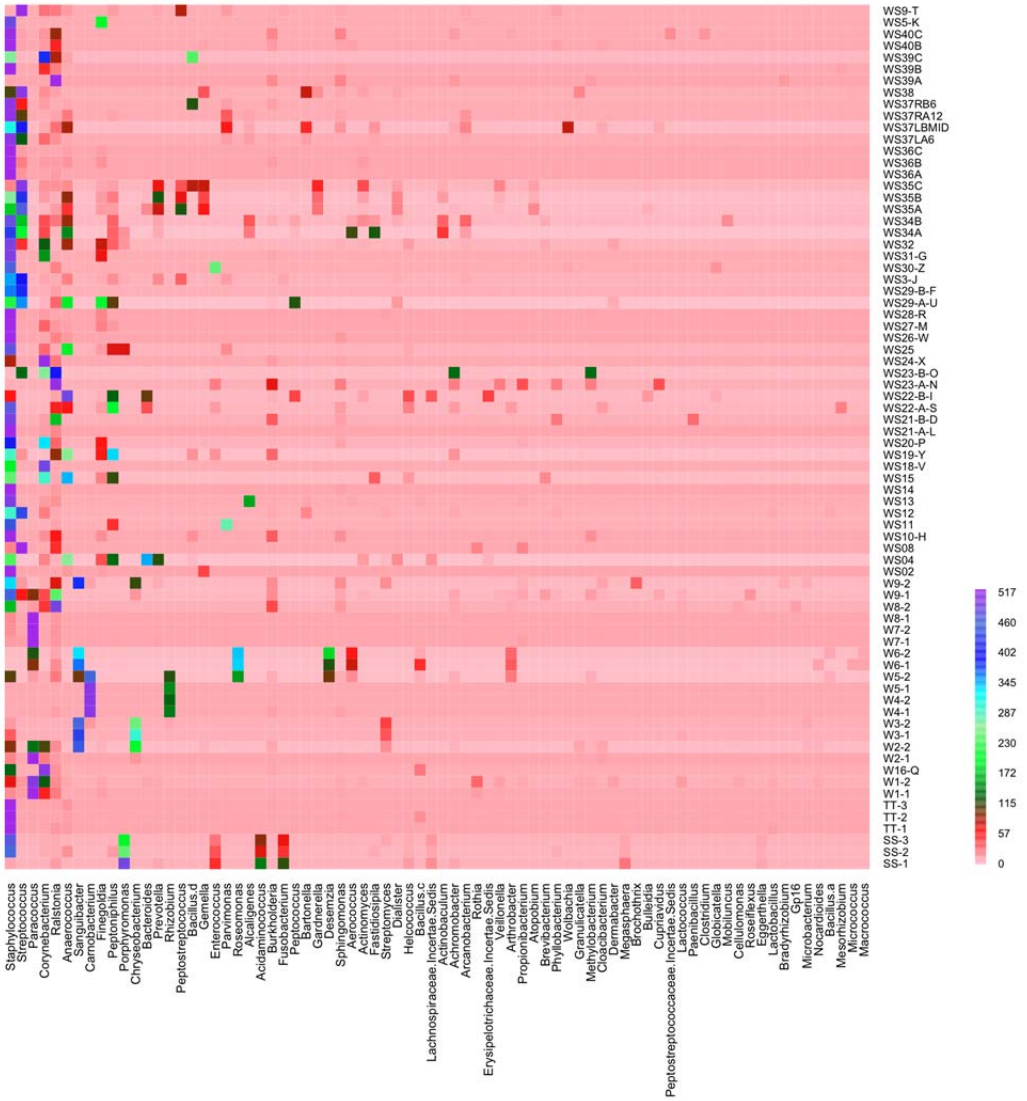

Figure 4. Heat Map Display of Genus-Level Phylotypes within Chronic Wound Samples.

Table 4. Seventy-six family-level phylotypes identified among the 74 chronic wound samples collected at the Johns Hopkins Wound Center.

Family	No. wound samples positive	Ave. copy number per positive	Total no. sequences (39,220 total)
Staphylococcaceae	67	172	11542
Pseudomonadaceae	67	89	5969
Rhodobacteraceae	13	209	2721
Streptococcaceae	32	82	2612
Enterobacteriaceae	54	36	1918
Clostridiales IS XI	44	41	1820
Corynebacteriaceae	46	40	1817
Burkholderiaceae	66	18	1183
Xanthomonadaceae	40	22	888
Carnobacteriaceae	11	66	729
Moraxellaceae	46	15	676
Sanguibacteraceae	7	96	675
Neisseriaceae	5	128	641
Micrococcaceae	28	18	512
Oxalobacteraceae	42	12	493
Bacillaceae	21	19	398
Rhizobiaceae	6	62	369
Flavobacteriaceae	12	30	364
Porphyromonadaceae	8	43	343
Bacteroidaceae	8	25	196
Prevotellaceae	12	16	196
Veillonellaceae	16	11	179
Peptostreptococcaceae	6	28	170
Enterococcaceae	16	10	159
Alcaligenaceae	29	5	144
Bacillales IS XI	7	19	135
Acetobacteraceae	3	41	122
Comamonadaceae	33	3	107
Planococcaceae	5	21	105
Actinomycetaceae	19	5	100
Campylobacteraceae	9	10	90
Fusobacteriaceae	5	15	75
Lachnospiraceae	9	8	72
Peptococcaceae	5	14	71
Bartonellaceae	5	13	65
Bifidobacteriaceae	5	12	61
Sphingomonadaceae	30	2	60
Aerococcaceae	9	6	58
Desulfovibrionaceae	3	17	51
Ruminococcaceae	7	7	49
Erysipelotrichaceae	6	8	48
Microbacteriaceae	11	4	48
Streptomycetaceae	9	5	47
Aeromonadaceae	20	2	46
Phyllobacteriaceae	12	2	29
Burkholderiales IS 5	15	1	20
Coriobacteriaceae	6	3	18
Propionibacteriaceae	11	1	15
Pseudomonadales IS 6	5	3	14
Anaplasmataceae	2	7	13

Dermabacteraceae	4	3	13
Brevibacteriaceae	5	3	13
Methylobacteriaceae	9	1	12
Listeriaceae	1	8	8
Clostridiaceae	1	8	8
Bradyrhizobiaceae	6	1	8
Lactobacillaceae	5	1	7
Paenibacillaceae	1	5	5
Chloroflexaceae	1	4	4
Acidobacteriaceae	2	2	4
Cellulomonadaceae	2	2	4
Geodermatophilaceae	2	2	4
Caulobacteraceae	4	1	4
Flexibacteraceae	2	2	3
Halomonadaceae	2	2	3
Nocardioidaceae	3	1	3
Planctomycetaceae	3	1	3
Rubrobacteraceae	1	2	2
Legionellaceae	1	2	2
Sphingobacteriaceae	2	1	2
Deinococcaceae	2	1	2
Kineosporiaceae	1	1	1
Nakamurellaceae	1	1	1
Williamsiaceae	1	1	1
Crenotrichaceae	1	1	1
Thermaceae	1	1	1

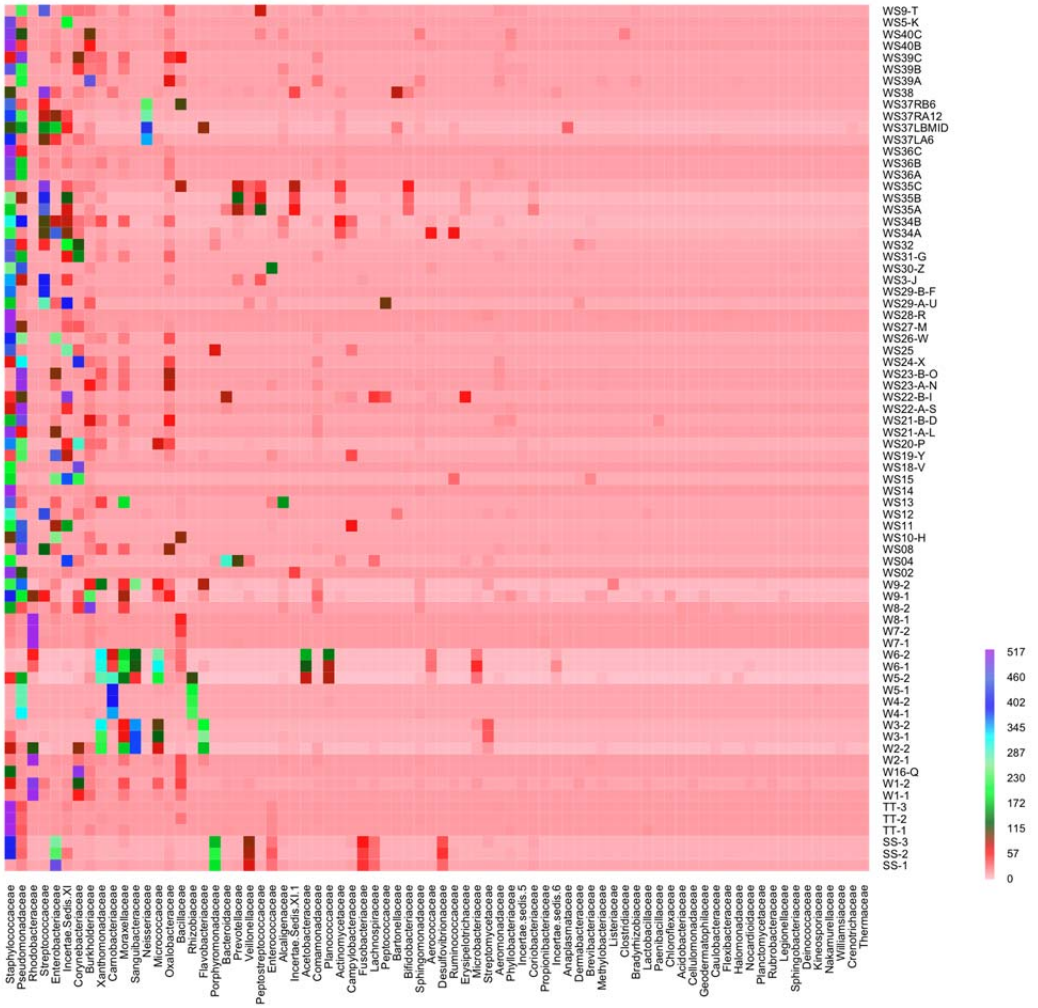

Figure 5. Heat Map Display of Family-Level Phylotypes within Chronic Wound Samples.

II.8. Engineered qPCR assays for the rapid detection of clinical pathogens

Bacterial species relevant to wound management were chosen to be targets for real-time PCR assays. The seven bacteria chosen were *Acinetobacter baumannii, Klebsiella pneumoniae, Escherichia coli, Pseudomonas aeruginosa, Aeromonas hydrophilia, Staphylococcus aureus* and *Shigella spp.* (required to differentiate *E. coli*). Of the seven assays, four were designed in-house and three were derived from the published literature. These assays were optimized and validated to be run on the LightCycler ® 480 Real Time PCR Instrument (Roche). The assay development processes are as follows:

A) *P. aeruginosa*: Thorough literature review one candidate assay was found. The regA (PMID: 17462712) assay was first optimized across a $MgCl_2$ gradient and different master mixes using positive control (*Psuedomonas aeruginosa* ATCC 27853) and no-template control. Preliminary specificity was tested using a small diverse panel.

B) *A. hydrophilia*: Thorough literature review one candidate assay was found. The aha1 (PMID: 17462712) assay was first optimized across a $MgCl_2$ gradient and different master mixes using positive control (*Aeromonas hydrophila* ATCC 35654) and no-template control. Preliminary specificity was tested using a small diverse panel.

C) *K. pneumoniae*: Thorough literature review two candidate assays were found. The WaaQ and phoE assays were first optimized across a $MgCl_2$ gradient and different master mixes using positive control (*Klebsiella pneumoniae subsp. pneumoniae* ATCC 13883) and no-template control. Preliminary specificity was tested using a small diverse panel. Due to assay performance and cross-reaction with non-target samples an in-house assay was designed and optimized in the same manner. The in-house WaaQ assay was then run across a larger set of *K. pneumoniae* samples to better determine the sensitivity.

D) *E. coli*: Thorough literature review one candidate assay was found. The uidA (PMID: 17462712) assay was first optimized across a $MgCl_2$ gradient and different master mixes using positive control

(*Escherichia coli* ATCC 25922) and no-template control. Preliminary specificity was tested using a small diverse panel. The assay was run across a larger set of *E. coli* and near-neighbor samples to better determine the sensitivity and specificity. It was observed that the *E. coli* uidA assay amplified both *E. coli* and *Shigella species*; consequently a *Shigella spp.* assay was designed to accompany the *E. coli* uidA assay.

E) *Shigella spp.*: Thorough literature review the ipaH gene was found to be a possible target for design of an in-house *Shigella spp.* assay. The ipaH assay was first optimized across a $MgCl_2$ gradient and different master mixes using positive control (*Shigella sonnei* genomic DNA) and no-template control. Preliminary specificity was tested using a small diverse panel.

F) *Acinetobacter baumannii*: Thorough literature review two candidate assay were found. The gyrB and BLA-OXA-51-like assays were first optimized across a $MgCl_2$ gradient and different master mixes using positive control (*Acinetobacter baumannii* ATCC 19606) and no-template control. Preliminary specificity was tested using a small diverse panel. Due to assay performance an in-house blaOXA51 assay was designed and optimized in the same manner.

G) *S. aureus*: An in-house femA assay was first optimized across a $MgCl_2$ gradient and different master mixes using positive control (*Staphylococcus aureus subsp. aureus* ATCC 29213) and no-template control. Preliminary specificity was tested using a small diverse panel. The assay was run across a larger set of *S. aureus* and near-neighbor samples to better determine the sensitivity and specificity. Although femA is an established target for *S. aureus,* it was determined that the assay was not *S. aureus* specific. Improvement and validation for the assay are ongoing, including sequence confirmation of the non-specific targets that appear to cross-react.

All assays were tested against panels of DNAs from near-neighbors and other clinically relevant bacterial species.

II.9. Quantify major phylotypes.

When we first composed this proposal, we planned to quantify phylotypes by qPCR; however, as we progressed, we found that we could use the number of pyrosequences to derive relative quantities of the different phylotypes. See **Table 3 & 4** and **Figures 4 & 5**.

II.10. Spatial Variation in Wounds

We analyzed spatial variation in wound microbiota using molecular tools and methods developed previously under this award.

Methods

Sample collection. Samples were taken from two to three sites from each of 13 wounds: site A, the leading edge of the wound; site B, the opposing leading edge; and/or site C, the wound center. TG02 and TG03 were sampled from a single site. Samples from TG02 and TG03 were frozen then each divided into three approximately equal portions. Each portion was processed and analyzed separately as technical replicates.

DNA extraction and purification. Genomic DNA was extracted from curette samples using a bead-beating and enzymatic lysis protocol, followed by purification using a QIAamp DNA Mini Kit (Qiagen, Valencia, USA). Briefly, the frozen tissue samples were thawed on ice and 0.75 ml of TE50 (10mM Tris-HCl + 50mM EDTA, pH 8.0) solution added. 500 µl of the solution was transferred to a clean, sterile bead-beating tube (MP Biomedicals, Solon, USA) and kept on ice. A lytic enzyme cocktail was prepared at the time of extraction and added to each sample as follows: 50 µl Lysozyme (450 kU ml-1), 6 µl Mutanolysin (25 kU ml-1), 3 µl Lysostaphin (4 kU ml-1) and 41 µl TE50 for a final volume of 100 ml per sample. Samples were digested by incubating at 37°C for 60 min in a dry heat block before centrifugation at 1200 rpm for 1 min. To each digested sample, 750 mg of sterile 0.1 mm diameter zirconia silica beads (BioSpec Products Inc., Bartlesville, USA) were added. Bead-beating was performed for 1 min at 2100 rpm using a BioSpec Mini-Bead Beater-96. Following bead disruption, the tubes were centrifuged at 1200 rpm for 1 min. Two 200 ml aliquots of crude lysate from each sample were transferred to new, sterile microcentrifuge tubes. To each tube, 25 µl of Proteinase K (20 mg/ml (>600 mAU/ml)) and 200 µl of Qiagen buffer AL were added. Samples were mixed by pulse-vortexing for 15 sec and then incubated at 56°C for 10 min before being centrifuged at 1200 rpm for 1 min. For each 200 µl crude lysate, 20 µl of 3 M sodium acetate, pH 5.5 was added followed by 200 µl of molecular grade ethanol (96–99.5%). Vortexing was repeated for an additional 15 sec before being centrifuged at 1200 rpm for 1 min. From this point onward, purification was carried out using the QIAmp DNA Purification

from Blood or Body Fluids as per manufacturer's instructions. Aliquots from the same sample were loaded onto the same column. Purified genomic DNA was stored at -80°C until analysis.

Pyrosequencing analysis of the 16S rRNA gene V3-V4 region for parallel tagged sequencing on the 454® platform. The 16S rRNA gene was amplified in two replicate 15 µl reaction volumes. In each 15 µl reaction, 1 µl was added to 14 µl of PCR reaction mix containing 450 nM of each broad range forward (5'-CCATCTCATCCCTGCGTGTCTCCGACTCAG-nnnnnnnnnn-CCTACGGGDGGCWGCA-3') and reverse primer (5'- CCTATCCCCTGTGTGCCTTGGCAGTCTCA-GGGACTACHVGGGTMTCTAATC-3'), 1X PCR buffer without $MgCl_2$ (Invitrogen, Carlsbad, USA), 3 mM $MgCl_2$, 0.2 mM dNTP mix, 1 U platinum *Taq* (Invitrogen) using the following touch-down PCR condition: 90s at 95°C for initial denaturation and 20 cycles of 30s at 95°C for denaturation, 30s at 60°C for annealing, 30s at 72°C for extension with the annealing temperature decreasing by 0.5°C for each subsequent cycle for followed by 10 cycles of 30s at 95°C for denaturation, 30s at 45°C for annealing, and 30s at 72°C for extension, and a final extension for 7 min at 72°C. The final tagged PCR products were then purified using the Agencourt® AMPure® Kit (Agencourt, Beverly, USA). Gel electrophoresis was performed using 5ul of the purified PCR product using the E-Gel® 96-well System (Invitrogen, Carlsbad, USA) for quality check and gel-based quantification. A second quantification was performed using an in-house 16S rRNA gene quantitative real-time PCR assay. The PCR products were then pooled in an equimolar fashion to generate the amplicon library for pyrosequencing. The emulsion PCR and pyrosequencing analysis using a Roche 454 XLR Titanium chemistry on the FLX pyrosequencer was performed according to the manufacturer instructions (454 Life Sciences, Branford, USA) at the Institute for Genome Sciences of University of Maryland.

Pyrosequencing data processing. Experimental sequences were processed using a custom PERL script, which performed the following: the script filtered the sequence files and retained only sequences that were 200-nt or longer. Regular expressions were then applied to the remaining sequences to search for a single barcode sequence in each FASTA sequence, binned each sequence accordingly, and scanned each binned sequence for the 16S forward primer sequence. The script then trimmed off the forward primer sequence and oriented the remaining sequence such that all sequences begin with the 5' end according to standard sense strand conventions. As a result of our processing, sequences that were shorter than 200-nt or had multiple barcode or primer motifs were excluded from the analysis.

Subset generation and taxonomic assignment. We evaluated the sequencing coverage by examining the number of 16S rRNA gene sequences generated per swab sample, which showed that the lowest number of sequences per sample to be n = 530. To facilitate subsequent phylotype abundance-based analyses, we standardized/normalized the number of sequences per swab sample to n = 530 sequences by sampling randomly without replacement prior to taxonomic classification to generate a single subset. We repeated this process four more times to generate a total of five subsets for confirmatory data analyses. Samples with less than n = 530 sequences were excluded. We classified the 16S rRNA gene sequences in each subset at each taxonomic level *(i.e.,* phylum, class, order, family, genus) at three bootstrap confidence levels: ≥95%, ≥97%, ≥99% using a web service for the Naïve Bayesian Classifier made available by the Ribosomal Database Project. An SQL database was used to store and query the results. To control for potential errors due to pyrosequencing that may have created rare phylotypes, we removed all family-level phylotypes occurring only once (i.e., singletons) in the dataset, the estimated equivalent of a proportional abundance of 1/530 = 0.19% in a single sample or 1/(530*31) = 0.0061% in the full dataset. The phylotype abundance data was converted into a data matrix in R, which we converted to a proportional abundance data matrix calculated by dividing the phylotype abundance by the total number of sequences assigned to the family-level in each sample. We assessed the potential biases of the subset generation approach by analyzing all five subsets classified at ≥95%, ≥97%, and ≥99% bootstrap confidence levels and found the variation among the subsets and different classification cutoffs to be non-significant. Subsequently, all data presented in the manuscript were derived from Subset 1 classified at 95% confidence level.

Visualization of the wound microbiota data. Subsequent data visualization and analyses were performed in R version 2.9.1 unless otherwise specified. We visualized the wound microbioa using two different approaches: 1) a heatmap display and 2) non-metric multi-dimensional scaling (nMDS). Heatmap display. We visually assessed the wound microbiota using a heatmap display in the vegan package (**Figure 6**). Non-metric

multidimensional scaling (nMDS) analysis. We utilized nMDS ordination to visually assess patterns microbiota compositional differences among our samples. All nMDS plots were generated in R using functions from ecodist, ellipse, and BiodiversityR. The Bray-Curtis distance was used for its excellent properties when used with community data. To generate each nMDS plot, we began by evaluating the number of dimensions required to appropriately present the bacterial communities using a stress plot, which was generated using n = 10 iterations of nMDS for dimensions n = 1 through n = 5. We applied a conventional cutoff of < 0.2 to determine the acceptable number of dimensions. Using the appropriate number of dimensions n = 50 iterations, Using the appropriate number of dimensions, the nMDS procedure was repeated with n = 50 iterations to more fully explore the ordination space at that dimensionality. The minimum stress solution from this was used to produce the nMDS plots in which each data point represents the bacterial community found in one sample. The spatial distance between points in the plot can be interpreted as the relative difference in community composition, hence, points that are closer are more similar than points that are more distant.

Multivariate ecological analyses. Due to the high level of similarity between the microbiota data matrix in the current study to ecological community data matrices, we chose to apply multivariate analysis methods typically used for ecological community data to assess the chronic wound microbiota. Ecology-type community data, which can be non-normal, zero-rich, and highly skewed—such as our current dataset—often require special analytical methods; this has been investigated and discussed thoroughly in the ecology literature. Permutation Multivariate Analysis of Variance (PerMANOVA). We used PerMANOVA to test the null-hypothesis of no-difference between the bacterial communities found within a single wound compared to those from different patients ($\alpha = 0.05$). PerMANOVA is a permutation-based version of the multivariate analysis of variance (MANOVA). PerMANOVA uses the distances between samples to partition variance and randomizations or permutations of the data to produce the p-value for the hypothesis test. It is non-parametric (or semi-parametric for multi-factor models) and, therefore, robust to the assumption of multivariate normality making it less prone to Type I errors. All PerMANOVA analyses were performed in R using the “adonis” function from the *vegan* package.

Results and Discussion

Heatmap display of wound microbiota revealed the diversity of microbial communities characterized in this study. A total of 51 bacterial families (Average 14 per wound; SD 4; Range 4 to 24) were represented in the 13 wounds analyzed (**Figure 6**). In general, samples from different sites within the same wounds showed similar diversity patterns; however, even technical replicate sets generated by dividing the same curette sample into three equal pieces showed some community variation.

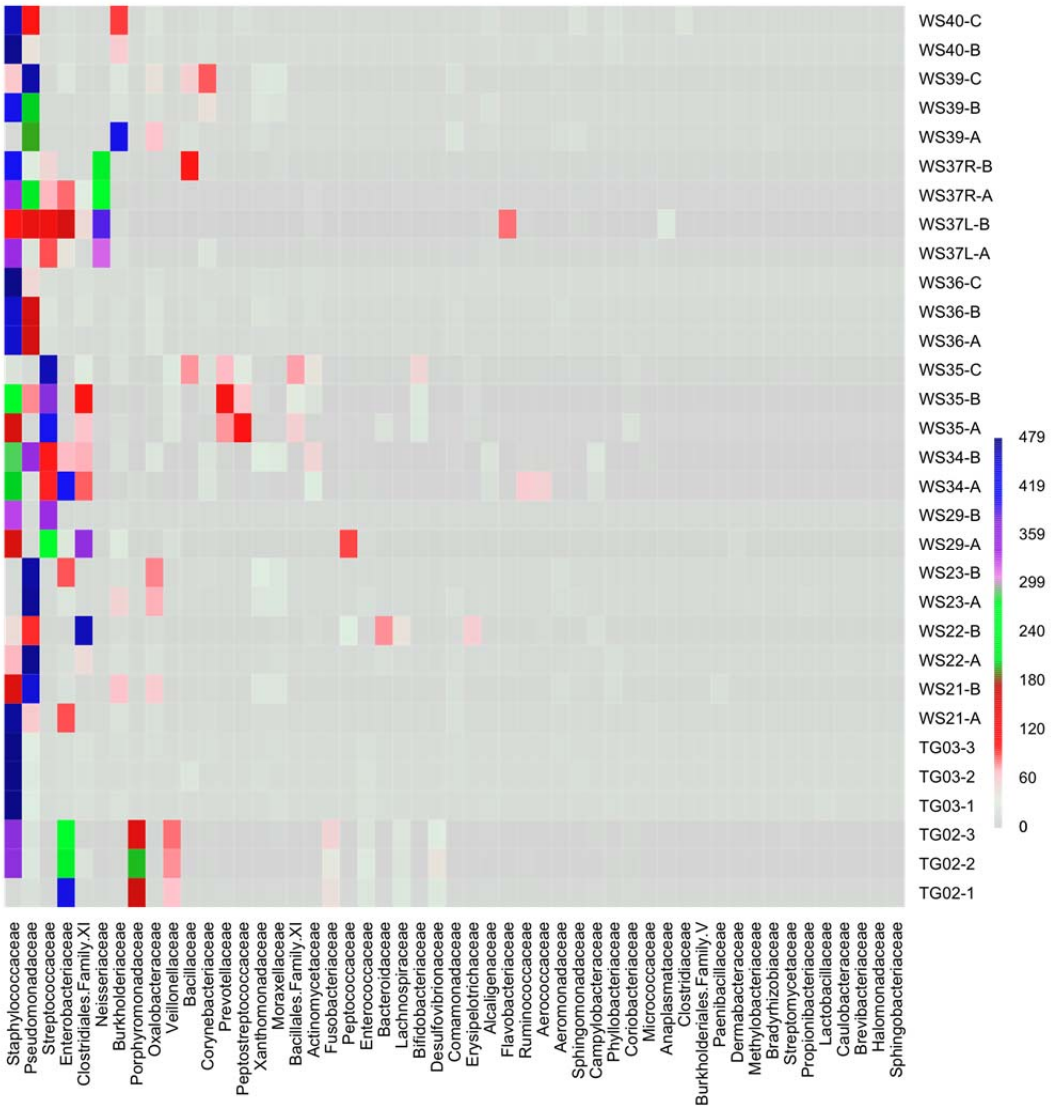

Figure 6A. Heatmap display of wound samples taken from different sites within the wounds (samples are grouped by wound). The color key for the number of sequences from each bacterial family is shown on the right. A = leading edge; B = apposing leading edge; C = center; TG02 and TG03 are technical replicates created by dividing a single curette sample into three equal parts prior to processing.

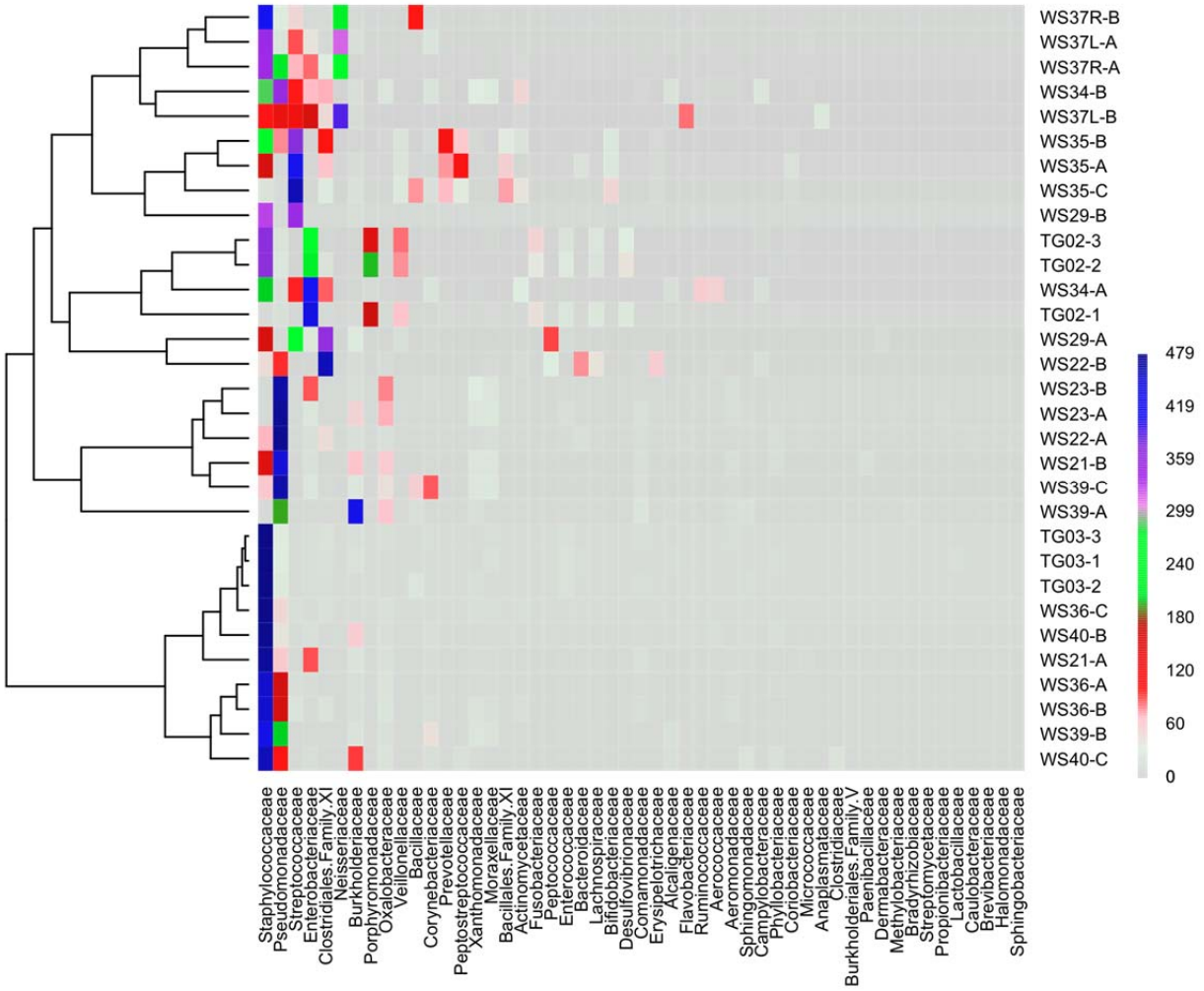

Figure 6B. Heatmap display of wound samples taken from different sites within the wounds (samples are grouped based on hierarchical clustering). The color key for the number of sequences from each bacterial family is shown on the right. A = leading edge; B = apposing leading edge; C = center; TG02 and TG03 are technical replicates created by dividing a single curette sample into three equal parts prior to processing.

In order to visualize relationships between bacterial communities within individual wound as well as between different wounds, we plotted samples using nMDS (**Figure 7**). This plot showed that samples taken from within an individual wound were more similar than those taken from different wounds. This finding was confirmed using perMANOVA analysis, which revealed that within-wound variation was significantly less than between-wound variation ($p = 0.001$). Samples from opposing leading edges did not appear to be any more similar than those from the center of the wound. Likewise, while one technical replicate set from a single site formed an extremely tight cluster, the other technical replicate set appeared to be as different as samples taken from different sites within a single wound.

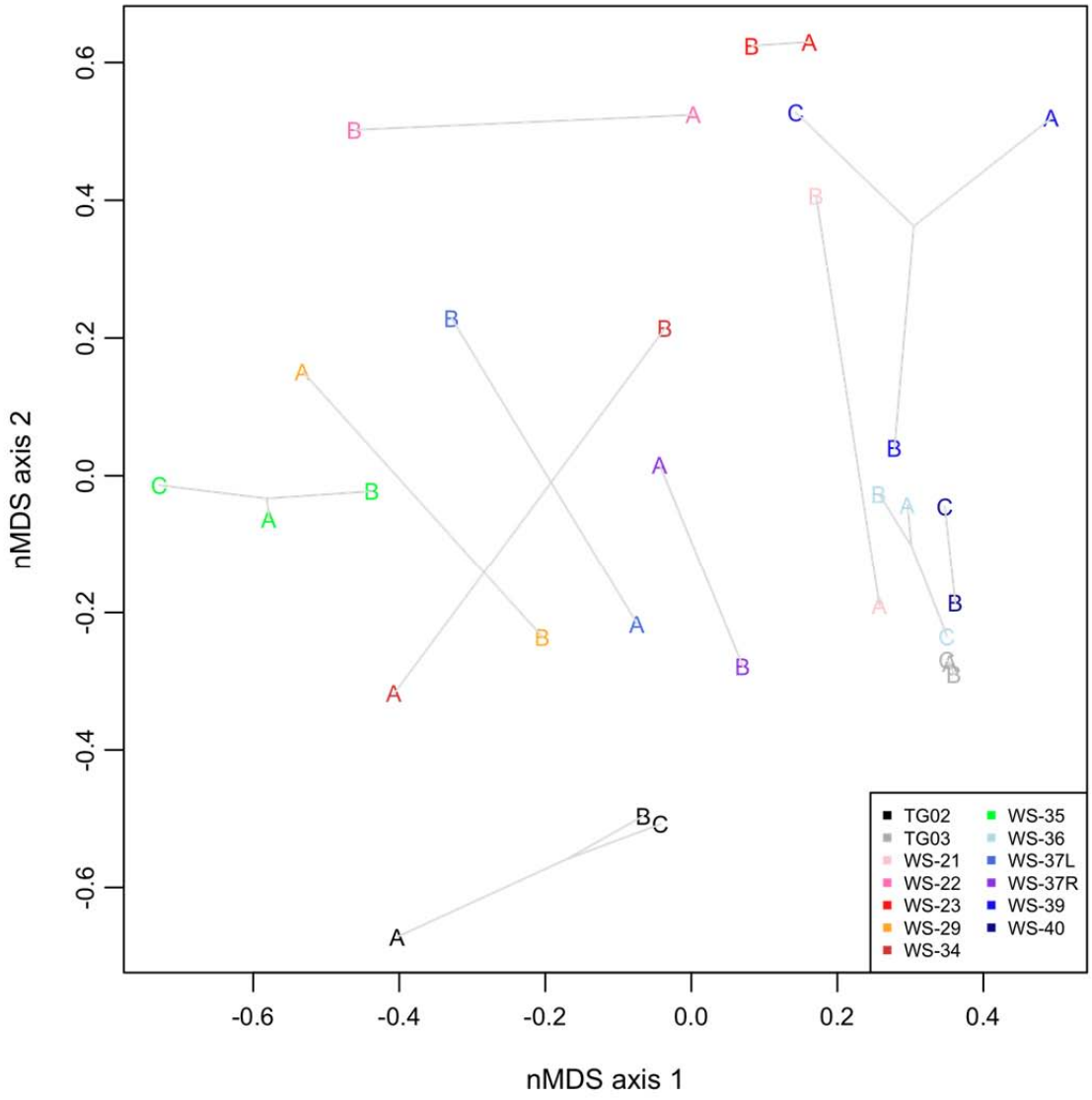

Figure 7. Non-metric Multi-Dimensional Scaling (nMDS) plot of wound samples taken from different sites within the wounds. A = leading edge; B = apposing leading edge; C = center; TG02 and TG03 are technical replicates created by dividing a single curette sample into three equal parts prior to processing.

Our results support the common opinion that controlling for sample site will improve the quality of wound microbiota studies; however, the significant similarity of communities within wounds indicates that studies failing to control for sample site should not be considered invalid based on this sole criterion. A prospective study of community composition at multiple sites within a wound over time may further elucidate the importance of sample site variation in wound studies.

A homogenized composite sample from multiple sites within a wound may provide the most robust picture of a wound's microbial community. Creating a post-analysis composite of sequence data generated from multiple samples taken from the same wound may provide all the benefits of a physical homogenization while allowing for additional independent analyses of the different sites. The need to homogenize the entire sample (or data)—whether from one site or multiple—was further supported by the technical replicate data sets. Microbial communities were shown to vary substantially even within a single curette sample.

All of the samples included in this study were taken from relatively small wounds, thus additional studies will have to be conducted to determine if wound size plays a significant role in the spatial variation of wound communities.

II.11. Variation in wounds over time.

We prospectively characterized the wound microbiota among nine burn wound patients using the pyrosequencing technique that we developed under this award (**Figure 8**). We found that the wound microbiota was fairly consistent over time, but impacted by the use of antibiotics. We will prepare a manuscript of our findings this year.

Figure 8. Prospective analysis of burn wound colonization.

Patient 0012

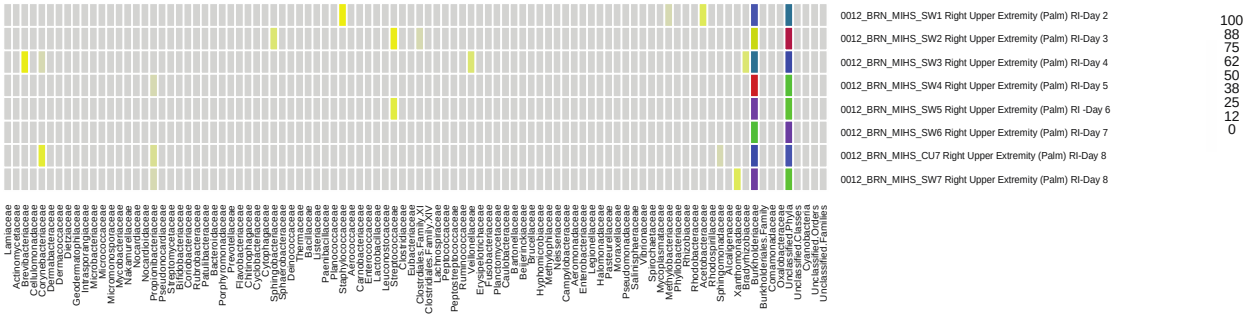

Patient 0011

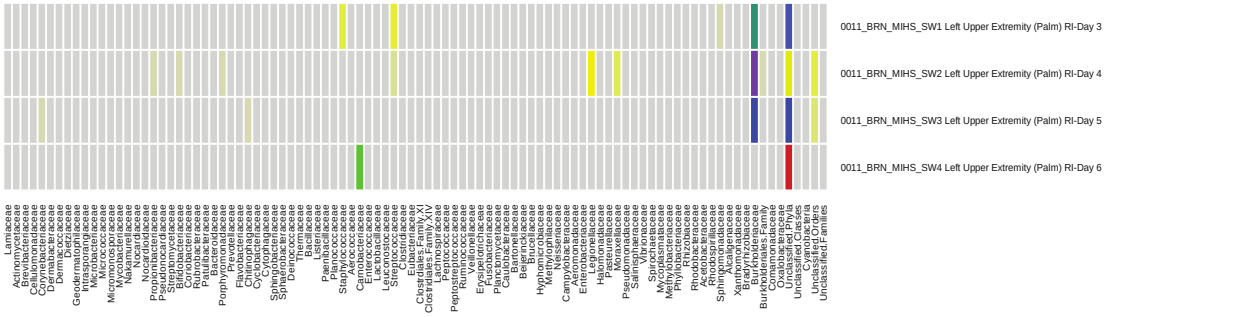

Patient 0010

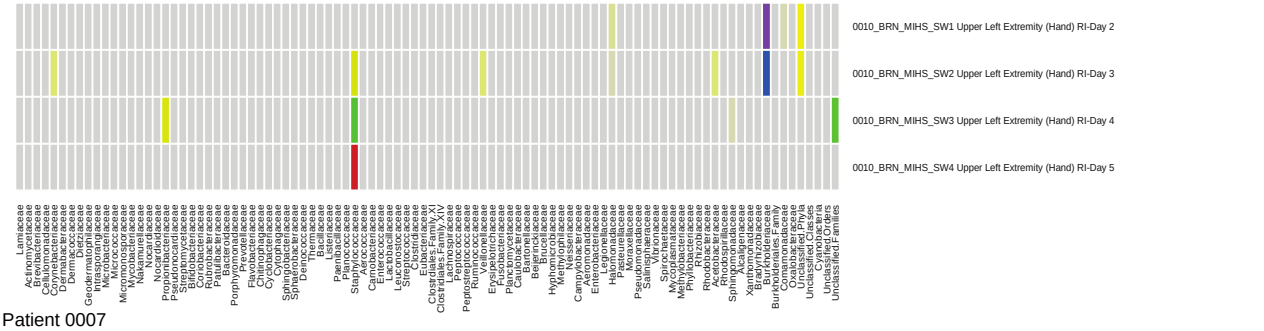

Patient 0007

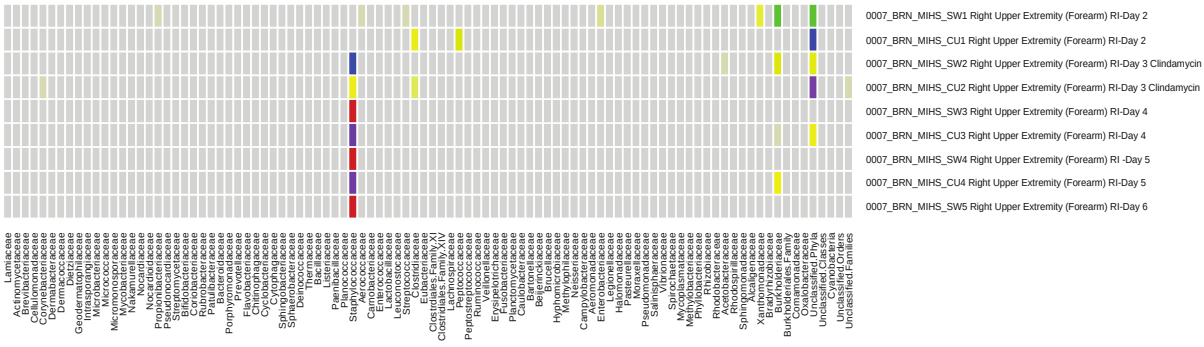

Patient 0005

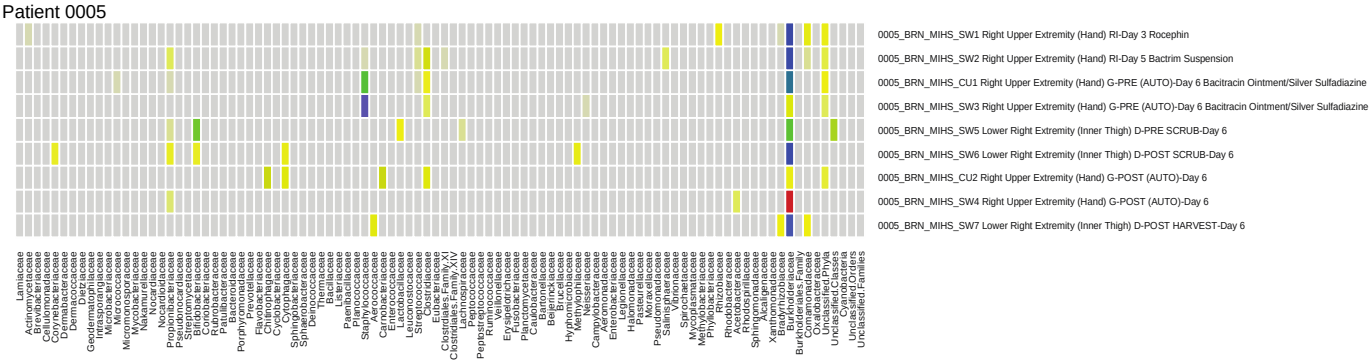

II.12. Established subcontracts with Maricopa Integrated Health Systems (MIHS)

TGen established subcontracts with MIHS to conduct prospective cohort studies: 1) burn wound colonization and outcomes; 2) chronic wound colonization and clinical response. MIHS is host to the Arizona Burn Center—the second largest burn unit in North America. They also have a chronic wound center on site and an active research team with whom we work closely to design robust clinical studies. The two groups have worked together to develop study consent forms, IRB applications, standard operating procedures, sample collection forms, etc. We received IRB approvals at both institutions and at the DoD to conduct the study.

II.13. Complete IRB submissions

All IRB applications were completed, submitted and approved at WIRB (TGen's IRB); MIHS; and Human Research Protection Office (HRPO).

II.14. Purchase and place equipment

All necessary equipment was purchased and placed at the two performance sites (TGen and MIHS).

II.15. Developed Database System for sample tracking and analysis

We developed web-based Laboratory Information Management System (LIMS) system that was designed to meet the specific needs of the TGen/MIHS prospective burn wound study funded under this award. The system was developed to facilitate tracking of information and materials transferred between TGen and the Arizona Burn Center at MIHS. Once logged into the system, each user has access to an interface customized to their particular needs. For example the "hospital" user (MIHS) can upload information about patient samples being collected, they can acknowledge receipts of collection kits from TGen, can notify TGen of samples being shipped, etc. The "biobank" user (TGen) can notify MIHS of collection kits being shipped, acknowledge receipt of burn wound samples from MIHS, upload information regarding analysis results, etc.

II.16. Collect and store burn wound samples

Over the course of this project we collected 721 burn wound samples from 71 patients enrolled into the study at the MIHS Arizona Burn Center.

II.17. Collect patient source samples

This objective was dropped due to the paucity of patients willing to participate.

II.18. Collect metadata

We collected relevant metadata on the patient as well as detailed burn wound characteristics as shown in **tables 5-8**. These data make the our sample repository an invaluable resource for studying burn wound healing into the future.

Table 5. Demographics.

Study Participant ID	Age	Sex	Ethnicity
0001-BRN-MIHS	63	Male	Native American; American Indian; Alaskan Native; or Inuit (Peoples of North; Central; or South America who maintain tribal affiliations or community attachment)
0002-BRN-MIHS	45	Male	African; African American; Caribbean Islander; or Black (Peoples of Africa or African descent)
0003-BRN-MIHS	48	Female	Middle Eastern; Arab American; Mediterranean (Peoples of North Africa and the Mediterranean)
0004-BRN-MIHS	18	Male	Native American; American Indian; Alaskan Native; or Inuit (Peoples of North; Central; or South America who maintain tribal affiliations or community attachment)
0005-BRN-MIHS	9	Female	Hispanic; Latina/Latino; Latin American (Peoples of Mexico; Puerto Rico; Cuba; or Central or South America; or of other Spanish cultures)
0006-BRN-MIHS	41	Male	Hispanic; Latina/Latino; Latin American (Peoples of Mexico; Puerto Rico; Cuba; or Central or South America; or of other Spanish cultures)

0007-BRN-MIHS	1	Female	European; European American; Caucasian or White (Peoples of Europe and North Africa)
0008-BRN-MIHS	50	Male	European; European American; Caucasian or White (Peoples of Europe and North Africa)
0009-BRN-MIHS	59	Male	European; European American; Caucasian or White (Peoples of Europe and North Africa)
0010-BRN-MIHS	19	Male	European; European American; Caucasian or White (Peoples of Europe and North Africa)
0011-BRN-MIHS	53	Male	European; European American; Caucasian or White (Peoples of Europe and North Africa)
0012-BRN-MIHS	53	Female	European; European American; Caucasian or White (Peoples of Europe and North Africa)
0013-BRN-MIHS	24	Male	European; European American; Caucasian or White (Peoples of Europe and North Africa)
0014-BRN-MIHS	30	Male	European; European American; Caucasian or White (Peoples of Europe and North Africa)
0015-BRN-MIHS	1	Male	Native American; American Indian; Alaskan Native; or Inuit (Peoples of North; Central; or South America who maintain tribal affiliations or community attachment)
0016-BRN-MIHS	5	Male	Hispanic; Latina/Latino; Latin American (Peoples of Mexico; Puerto Rico; Cuba; or Central or South America; or of other Spanish cultures)
0017-BRN-MIHS	52	Male	European; European American; Caucasian or White (Peoples of Europe and North Africa)
0018-BRN-MIHS	1	Male	Hispanic; Latina/Latino; Latin American (Peoples of Mexico; Puerto Rico; Cuba; or Central or South America; or of other Spanish cultures)
0019-BRN-MIHS	24	Female	European; European American; Caucasian or White (Peoples of Europe and North Africa)
0020-BRN-MIHS	57	Male	African; African American; Caribbean Islander; or Black (Peoples of Africa or African descent)
0021-BRN-MIHS	28	Male	European; European American; Caucasian or White (Peoples of Europe and North Africa)
0022-BRN-MIHS	44	Male	European; European American; Caucasian or White (Peoples of Europe and North Africa)
0023-BRN-MIHS	3	Female	European; European American; Caucasian or White (Peoples of Europe and North Africa)
0024-BRN-MIHS	19	Male	African; African American; Caribbean Islander; or Black (Peoples of Africa or African descent)
0025-BRN-MIHS	41	Male	Hispanic; Latina/Latino; Latin American (Peoples of Mexico; Puerto Rico; Cuba; or Central or South America; or of other Spanish cultures)
0026-BRN-MIHS	53	Female	European; European American; Caucasian or White (Peoples of Europe and North Africa)
0027-BRN-MIHS	41	Male	Hispanic; Latina/Latino; Latin American (Peoples of Mexico; Puerto Rico; Cuba; or Central or South America; or of other Spanish cultures)
0028-BRN-MIHS	2	Male	African; African American; Caribbean Islander; or Black (Peoples of Africa or African descent)
0029-BRN-MIHS	42	Male	European; European American; Caucasian or White (Peoples of Europe and North Africa)
0030-BRN-MIHS	38	Male	Hispanic; Latina/Latino; Latin American (Peoples of Mexico; Puerto Rico; Cuba; or Central or South America; or of other Spanish cultures)
0031-BRN-MIHS	37	Female	African; African American; Caribbean Islander; or Black (Peoples of Africa or African descent)
0032-BRN-MIHS	21	Female	Hispanic; Latina/Latino; Latin American (Peoples of Mexico; Puerto Rico; Cuba; or Central or South America; or of other Spanish cultures)
0033-BRN-	23	Male	European; European American; Caucasian or White (Peoples of Europe

MIHS			and North Africa)
0034-BRN-MIHS	32	Female	Hispanic; Latina/Latino; Latin American (Peoples of Mexico; Puerto Rico; Cuba; or Central or South America; or of other Spanish cultures)
0035-BRN-MIHS	29	Male	Hispanic; Latina/Latino; Latin American (Peoples of Mexico; Puerto Rico; Cuba; or Central or South America; or of other Spanish cultures)
0036-BRN-MIHS	15	Male	Hispanic; Latina/Latino; Latin American (Peoples of Mexico; Puerto Rico; Cuba; or Central or South America; or of other Spanish cultures)
0037-BRN-MIHS	29	Male	European; European American; Caucasian or White (Peoples of Europe and North Africa)
0038-BRN-MIHS	15	Male	European; European American; Caucasian or White (Peoples of Europe and North Africa)
0039-BRN-MIHS	10	Male	European; European American; Caucasian or White (Peoples of Europe and North Africa)
0040-BRN-MIHS	30	Male	European; European American; Caucasian or White (Peoples of Europe and North Africa)
0042-BRN-MIHS	26	Male	European; European American; Caucasian or White (Peoples of Europe and North Africa)
0043-BRN-MIHS	56	Female	European; European American; Caucasian or White (Peoples of Europe and North Africa)
0044-BRN-MIHS	8	Male	European; European American; Caucasian or White (Peoples of Europe and North Africa)
0045-BRN-MIHS	34	Male	European; European American; Caucasian or White (Peoples of Europe and North Africa)
0046-BRN-MIHS	52	Male	European; European American; Caucasian or White (Peoples of Europe and North Africa)
0047-BRN-MIHS	0.1	Male	Hispanic; Latina/Latino; Latin American (Peoples of Mexico; Puerto Rico; Cuba; or Central or South America; or of other Spanish cultures)
0048-BRN-MIHS	27	Male	Hispanic; Latina/Latino; Latin American (Peoples of Mexico; Puerto Rico; Cuba; or Central or South America; or of other Spanish cultures)
0049-BRN-MIHS	52	Male	European; European American; Caucasian or White (Peoples of Europe and North Africa)
0050-BRN-MIHS	28	Female	European; European American; Caucasian or White (Peoples of Europe and North Africa)
0051-BRN-MIHS	7	Male	European; European American; Caucasian or White (Peoples of Europe and North Africa)
0052-BRN-MIHS	36	Male	Asian or Asian American (Peoples of the Far East; Southeast Asia; or the Indian subcontinent)
0053-BRN-MIHS	2	Female	Native American; American Indian; Alaskan Native; or Inuit (Peoples of North; Central; or South America who maintain tribal affiliations or community attachment)
0054-BRN-MIHS	24	Male	European; European American; Caucasian or White (Peoples of Europe and North Africa)
0055-BRN-MIHS	36	Male	African; African American; Caribbean Islander; or Black (Peoples of Africa or African descent)
0056-BRN-MIHS	18	Female	European; European American; Caucasian or White (Peoples of Europe and North Africa)
0057-BRN-MIHS	22	Male	European; European American; Caucasian or White (Peoples of Europe and North Africa)
0058-BRN-MIHS	22	Male	European; European American; Caucasian or White (Peoples of Europe and North Africa)
0059-BRN-MIHS	67	Female	European; European American; Caucasian or White (Peoples of Europe and North Africa)
0060-BRN-MIHS	5	Female	Hispanic; Latina/Latino; Latin American (Peoples of Mexico; Puerto Rico; Cuba; or Central or South America; or of other Spanish cultures)

0061-BRN-MIHS	3	Female	Native American; American Indian; Alaskan Native; or Inuit (Peoples of North; Central; or South America who maintain tribal affiliations or community attachment)
0062-BRN-MIHS	25	Female	European; European American; Caucasian or White (Peoples of Europe and North Africa)
0063-BRN-MIHS	22	Male	Middle Eastern; Arab American; Mediterranean (Peoples of North Africa and the Mediterranean)
0065-BRN-MIHS	49	Male	European; European American; Caucasian or White (Peoples of Europe and North Africa)
0066-BRN-MIHS	18	Male	European; European American; Caucasian or White (Peoples of Europe and North Africa)
0067-BRN-MIHS	48	Male	N/A
0068-BRN-MIHS	25	Male	African; African American; Caribbean Islander; or Black (Peoples of Africa or African descent)
0069-BRN-MIHS	61	Male	European; European American; Caucasian or White (Peoples of Europe and North Africa)
0070-BRN-MIHS	22	Male	Hispanic; Latina/Latino; Latin American (Peoples of Mexico; Puerto Rico; Cuba; or Central or South America; or of other Spanish cultures)
0071-BRN-MIHS	6	Female	European; European American; Caucasian or White (Peoples of Europe and North Africa)

Table 6. Burn wound type and comorbidities.

Study Participant ID	Burn Mechanism	% Total BSA B	Depth of Burn	Coexisting Inhalation Injury	Other Comorbidities
0001-BRN-MIHS	Thermal: Flame	1	2nd Degree Superficial	No	Seizure disorder
0002-BRN-MIHS	Thermal: Flame	3	2nd Degree Superficial	No	NA
0003-BRN-MIHS	Thermal: Scald	NA	2nd Degree Superficial	No	Hypothyroidism
0004-BRN-MIHS	Thermal: Flame	2	2nd Degree Superficial	No	NA
0005-BRN-MIHS	Other: Contact Burn	1	Full Thickness	No	Urinary Tract Infection
0006-BRN-MIHS	Other: Grease Burn	2	2nd Degree Deep	No	Bipolar Depression
0007-BRN-MIHS	Thermal: Scald	10	2nd Degree Superficial	No	Asthma
0008-BRN-MIHS	Thermal: Flame	5	2nd Degree Superficial	No	Hypothyroidism
0009-BRN-MIHS	Electrical	1	2nd Degree Superficial	No	NA
0010-BRN-MIHS	Thermal: Scald	1	2nd Degree Superficial	No	Attention Deficit Disorder
0011-BRN-MIHS	Thermal: Flame	2	2nd Degree Superficial	No	Alcohol Dependence
0012-BRN-MIHS	Thermal: Scald	10	2nd Degree Deep	No	Hypothyroidism
0013-BRN-MIHS	Other: Contact/Grease	7.5	2nd Degree Deep	No	NA

	Burn				
0014-BRN-MIHS	Thermal: Flame	4	2nd Degree Deep	No	Diabetes
0015-BRN-MIHS	Other: Contact Burn	3	2nd Degree Deep	No	NA
0016-BRN-MIHS	Thermal: Scald	4	2nd Degree Superficial	No	NA
0017-BRN-MIHS	Thermal: Flame	13.5	2nd Degree Deep	No	Foot Surgery in 1980
0018-BRN-MIHS	Other: Contact Burn	2	2nd Degree Deep	No	NA
0019-BRN-MIHS	Thermal: Flame	9	2nd Degree Deep	Yes	NA
0020-BRN-MIHS	Thermal: Flame	NA	2nd Degree Superficial	No	NA
0021-BRN-MIHS	Thermal: Flame	5	2nd Degree Deep	No	NA
0022-BRN-MIHS	Thermal: Flame	13	2nd Degree Deep	No	NA
0023-BRN-MIHS	Other: Contact Burn	2	Full Thickness	No	NA
0024-BRN-MIHS	Other: Thermal: Contact Burn	3	Full Thickness	No	NA
0025-BRN-MIHS	Thermal: Scald	NA	2nd Degree Superficial	No	NA
0026-BRN-MIHS	Chemical Burn	4	2nd Degree Superficial	No	Hypothyroidism
0027-BRN-MIHS	Thermal: Flame	4	2nd Degree Superficial	No	Asthma/Obesity
0028-BRN-MIHS	Other: Thermal: Contact Burn	2	2nd Degree Deep	No	NA
0029-BRN-MIHS	Chemical Burn	3	2nd Degree Superficial	No	NA
0030-BRN-MIHS	Thermal: Flame	5	2nd Degree Deep	No	NA
0031-BRN-MIHS	Thermal: Flame	2	2nd Degree Deep	No	NA
0032-BRN-MIHS	Thermal: Flame	12	Full Thickness	No	None
0033-BRN-MIHS	Thermal: Flame	NA	Full Thickness	No	Coarctation of Aorta (repaired as a child)
0034-BRN-MIHS	Thermal: Scald	12	2nd Degree Superficial	No	None
0035-BRN-MIHS	Thermal: Flame	30	2nd Degree Deep	No	NA
0036-BRN-MIHS	Other: Contact Burn	1	Full Thickness	No	NA
0037-BRN-MIHS	Thermal: Flame	1	Full Thickness	No	Depression
0038-BRN-MIHS	Thermal: Scald	3	2nd Degree Deep	No	NA
0039-BRN-MIHS	Other: Friction Burn	NA	2nd Degree Superficial	No	NA
0040-BRN-	Thermal: Flame	10	2nd Degree Deep	No	NA

MIHS					
0042-BRN-MIHS	Thermal: Flame	1	2nd Degree Superficial	No	Seasonal Allergic Rhinitis
0043-BRN-MIHS	Thermal: Flame	26	2nd Degree Deep	No	A-fib; fibromyalgia; hypothyroidism; sciatia; CHF; aortic stenosis
0044-BRN-MIHS	Thermal: Flame	9	Full Thickness	No	NA
0045-BRN-MIHS	Thermal: Scald	1	2nd Degree Deep	No	Bipolar Depression
0046-BRN-MIHS	Thermal: Flame	3	2nd Degree Superficial	No	Multiple Sclerosis
0047-BRN-MIHS	Other: Contact Burn	1	Full Thickness	No	None
0048-BRN-MIHS	Other: Friction Burn (Road Rash)	4	2nd Degree Superficial	No	None
0049-BRN-MIHS	Thermal: Flame	5	2nd Degree Deep	No	NA
0050-BRN-MIHS	Thermal: Flame	4	2nd Degree Superficial	No	Herniated Disc
0051-BRN-MIHS	Thermal: Flame	4	Full Thickness	No	ADHD
0052-BRN-MIHS	Thermal: Flame	NA	Full Thickness	No	None
0053-BRN-MIHS	Thermal: Scald	6	2nd Degree Superficial	No	None
0054-BRN-MIHS	Thermal: Flame	9	2nd Degree Deep	No	None
0055-BRN-MIHS	Other: Contact Burn	8	Full Thickness	No	None
0056-BRN-MIHS	Thermal: Flame	NA	2nd Degree Deep	No	None
0057-BRN-MIHS	Thermal: Flame	4	Full Thickness	No	NA
0058-BRN-MIHS	Thermal: Flame	5	2nd Degree Deep	No	NA
0059-BRN-MIHS	Thermal: Scald	5	Full Thickness	No	TIA, Seizure, Bipolar Disorder, Fibromyalgia
0060-BRN-MIHS	Thermal: Scald	42	2nd Degree Deep	No	NA
0061-BRN-MIHS	NA	NA	NA	NA	NA
0062-BRN-MIHS	Unspecified	4	Full Thickness	No	Seizures
0063-BRN-MIHS	Thermal: Flame	9	2nd Degree Superficial	No	NA
0065-BRN-MIHS	Other: Friction Burn (Road Rash)	10	Full Thickness	No	NA
0066-BRN-MIHS	Thermal: Flame	5	2nd Degree Deep	No	Asthma
0067-BRN-	Other: Contact:	2	2nd Degree Superficial	No	NA

MIHS	Asphalt Burn				
0068-BRN-MIHS	Other: Friction Burn (Road Rash)	6	2nd Degree Superficial	No	NA
0069-BRN-MIHS	Thermal: Flame	7	2nd Degree Superficial	No	NA
0070-BRN-MIHS	Thermal: Scald	NA	2nd Degree Superficial	No	NA
0071-BRN-MIHS	Thermal: Scald	10	Full Thickness	No	NA

Table 7. Burn injury site.

Study Participant ID	Location of Burn Wound Sampled	Depth of Burn	Day Post-Injury at Initial Burn Wound Sample Collection
0001-BRN-MIHS	Right Upper Arm	2nd Degree Superficial	NA
0002-BRN-MIHS	Left Hand Dorsum	2nd Degree Superficial	NA
0003-BRN-MIHS	Upper Left Arm	2nd Degree Superficial	NA
0004-BRN-MIHS	Upper Right Extremity (Hand)	2nd Degree Superficial	NA
0005-BRN-MIHS	Right Upper Extremity (Hand)	Full Thickness	NA
0006-BRN-MIHS	Upper Right Extremity (Hand)	2nd Degree Deep	NA
0007-BRN-MIHS	Right Upper Extremity (Forearm)	2nd Degree Superficial	NA
0008-BRN-MIHS	Upper Right Extremity (Forearm)	2nd Degree Superficial	NA
0009-BRN-MIHS	Right Upper Extremity (Palm)	2nd Degree Superficial	NA
0010-BRN-MIHS	Upper Left Extremity (Hand)	2nd Degree Superficial	NA
0011-BRN-MIHS	Left Upper Extremity (Palm)	2nd Degree Superficial	Day 4 Post-Injury (5/30-6/3)
0012-BRN-MIHS	Right Upper Extremity (Palm)	2nd Degree Deep	Day 2 Post-Injury (6/5-6/7)
0013-BRN-MIHS	Left Hand	2nd Degree Deep	Day 2 Post-Injury (6/29-7/1)
0014-BRN-MIHS	Left Upper Arm	2nd Degree Deep	Day 2 Post-Injury (7/5-7/7)
0015-BRN-MIHS	Left Foot	2nd Degree Deep	Day 4 Post-Injury (7/4-7/8)
0016-BRN-MIHS	Abdomen	2nd Degree Superficial	Day 4 Post-Injury (7/10-7/14)
0017-BRN-MIHS	Left Forearm	2nd Degree Deep	Day 4 Post-Injury (7/30-8/3)
0018-BRN-MIHS	Left Hand	2nd Degree Deep	Day 7 Post-Injury (8/4-8/11)
0019-BRN-MIHS	Left Forearm	2nd Degree Deep	Day 3 Post-Injury (8/4-8/7)
0020-BRN-	Right Anterior Lower Extremity	2nd Degree Superficial	Day 2 Post-Injury (8/11-8/13)

MIHS			
0021-BRN-MIHS	Left Forearm	2nd Degree Deep	Day 4 Post-Injury (8/22-8/26)
0022-BRN-MIHS	Right Flank	2nd Degree Deep	Day 4 Post-Injury (9/4-9/8)
0023-BRN-MIHS	Left Forearm	Full Thickness	Day 2 Post-Injury (9/6-9/8)
0024-BRN-MIHS	Posterior Left Shoulder	Full Thickness	Day 4 Post-Injury (9/19-9/23)
0025-BRN-MIHS	Right Posterior Shoulder	2nd Degree Superficial	Day 4 Post-Injury (9/20-9/24)
0026-BRN-MIHS	Left Buttock	2nd Degree Superficial	Day 3 Post-Injury (10/3-10/6)
0027-BRN-MIHS	Left Side of Face	2nd Degree Superficial	Day 3 Post-Injury (10/10-10/13)
0028-BRN-MIHS	Left Medial Thigh	2nd Degree Deep	Day 2 Post-Injury (10/13-10/15)
0029-BRN-MIHS	Dorsum of Left Lower Foot	2nd Degree Superficial	Day 3 Post-Injury (10/17-10/20)
0030-BRN-MIHS	Lateral Aspect of Right Calf	2nd Degree Deep	Day 3 Post-Injury (10/25-10/28)
0031-BRN-MIHS	Right Hand	2nd Degree Deep	Day 2 Post-Injury (11/2-11/4)
0032-BRN-MIHS	Dorsum of Left/Right Hand	Full Thickness	Day 3 Post-Injury (11/6-11/9)
0033-BRN-MIHS	Dorsum of Right Hand	Full Thickness	Day 13 Post-Injury (11/17-11/30)
0034-BRN-MIHS	Left Breast	2nd Degree Superficial	Day 1 Post-Injury (12/1-12/2)
0035-BRN-MIHS	Anterior Torso	2nd Degree Deep	Day 2 Post-Injury (12/7-12/9)
0036-BRN-MIHS	Right Side of Face	Full Thickness	Day 3 Post-Injury (1/1-1/4)
0037-BRN-MIHS	Left Foot	Full Thickness	Day 3 Post-Injury (1/4-1/7)
0038-BRN-MIHS	Right Foot	2nd Degree Deep	Day 2 Post-Injury (1/13-1/15)
0039-BRN-MIHS	Posterior Trunk	2nd Degree Superficial	Day 2 Post-Injury (1/16-1/18)
0040-BRN-MIHS	Right Anterior Lower Leg	2nd Degree Deep	Day 2 Post-Injury (1/17-1/19)
0042-BRN-MIHS	Left Hand	2nd Degree Superficial	Day 3 Post-Injury (1/29-2/1)
0043-BRN-MIHS	Right Anterior Trunk	Full Thickness	Day 2 Post-Injury (2/6-2/8)
0044-BRN-MIHS	Right Anterior Lower Leg	Full Thickness	Day 3 Post-Injury (2/10-2/13)
0045-BRN-MIHS	Dorsum of Right Foot	2nd Degree Deep	Day 4 Post-Injury (2/12-2/16)
0046-BRN-MIHS	Right Posterior Trunk	2nd Degree Superficial	Day 2 Post-Injury (2/15-2/17)
0047-BRN-MIHS	Left Forearm	Full Thickness	Day 2 Post-Injury (2/16-2/18)
0048-BRN-	Right Anterior Lower Leg	2nd Degree Superficial	Day 1 Post-Injury (2/17-2/18)

MIHS			
0049-BRN-MIHS	Left Lower Leg	2nd Degree Deep	Day 3 Post-Injury (3/15-3/18)
0050-BRN-MIHS	Anterior Flank/Abdomen	2nd Degree Superficial	Day 2 Post-Injury (3/29-3/31)
0051-BRN-MIHS	Anterior Trunk/Torso	Full Thickness	Day 3 Post-Injury (3/30-4/2)
0052-BRN-MIHS	Right Side of Neck	Full Thickness	Day 3 Post-Injury (4/2-4/5)
0053-BRN-MIHS	Posterior Left Medial Calf	2nd Degree Superficial	Day 2 Post-Injury (4/7-4/9)
0054-BRN-MIHS	Left/Right Medial Lower Leg	2nd Degree Deep	Day 2 Post-Injury (4/10-4/12)
0055-BRN-MIHS	Left Anterior Chest/Torso	Full Thickness	Day 2 Post-Injury (4/14-4/16)
0056-BRN-MIHS	Right Forearm	2nd Degree Deep	Day 2 Post-Injury (4/17-4/19)
0057-BRN-MIHS	Left Foot	Full Thickness	4/23-NA
0058-BRN-MIHS	Right Forearm	2nd Degree Deep	Day 3 Post-Injury (4/23-4/26)
0059-BRN-MIHS	NA	Full Thickness	4/30-NA
0060-BRN-MIHS	Anterior Torso	2nd Degree Deep	Day 1 Post-Injury (5/11-5/12)
0061-BRN-MIHS	Right Lower Leg	NA	NA-5/24
0062-BRN-MIHS	Right Posterior Arm	Full Thickness	5/24-NA
0063-BRN-MIHS	Left Upper Arm	2nd Degree Superficial	5/24-NA
0065-BRN-MIHS	Posterior Right Upper Arm	Full Thickness	6/14-NA
0066-BRN-MIHS	Right Posterior Upper Arm	2nd Degree Deep	Day 2 Post-Injury (6/26-6/28)
0067-BRN-MIHS	Left Foot	2nd Degree Superficial	Day 2 Post-Injury (7/10-7/12)
0068-BRN-MIHS	Right Hand	2nd Degree Superficial	Day 3 Post-Injury (7/13-7/16)
0069-BRN-MIHS	Right Arm/Forearm	2nd Degree Superficial	Day 3 Post-Injury (7/23-7/26)
0070-BRN-MIHS	Left Arm	2nd Degree Superficial	Day 3 Post-Injury (7/23-7/26)
0071-BRN-MIHS	Anterior Torso	Full Thickness	Day 3 Post-Injury (8/6-8/9)

II.19. Monthly shipments MIHS to TGen

MIHS shipped burn wound samples to TGen on a near monthly basis or when a critical mass of samples necessitated more frequent delivery.

II.20. Pyrosequence samples

We pyrosequenced 399 burn wound samples. We had an unusually high number of sequencing failures due in part to the low bacterial load in burns as compared to chronic wounds; however, were able to generate

the prospective plots under section II.11 and below in II.22. We will continue to refine our techniques with analyzing low bacterial load samples into the future.

II.21. Clone library analysis

This objective was supplanted by pyrosequence library generation (as described previously).

II.22. Identify common phylotypes

Using pyrosequencing, we identified 99 bacterial families (**Table 10)** and 187 bacterial genera among the burn wound samples analyzed.

Table 8. Major burn wound phylogroups.

Family	Relative abundance
Staphylococcaceae	0.354240263
Bradyrhizobiaceae	0.22384412
Burkholderiaceae	0.084494212
Streptococcaceae	0.027550046
Pseudomonadaceae	0.023995201
Propionibacteriaceae	0.017663134
Corynebacteriaceae	0.016596681
Porphyromonadaceae	0.010509009
Comamonadaceae	0.009420338
Fusobacteriaceae	0.008176143
Sphingomonadaceae	0.00779844
Xanthomonadaceae	0.006643116
Enterococcaceae	0.005954365
Enterobacteriaceae	0.005421138
Flavobacteriaceae	0.004487991
Rhodobacteraceae	0.003888111
Prevotellaceae	0.003865893
Micrococcaceae	0.003754805
Incertae Sedis XI	0.003688151
Clostridiaceae	0.003665933
Spirochaetaceae	0.003554845
Moraxellaceae	0.003110489
Chitinophagaceae	0.002732787
Pasteurellaceae	0.00239952
Bacillaceae	0.002288431
Acetobacteraceae	0.001644116
Peptococcaceae	0.001533027
Veillonellaceae	0.001421938
Micromonosporaceae	0.001333067
Aerococcaceae	0.001221978
Campylobacteraceae	0.001155324
Cytophagaceae	0.001110889
Actinomycetaceae	0.001044236
Intrasporangiaceae	0.001044236

Planococcaceae	0.0009998
Neisseriaceae	0.000844276
Leuconostocaceae	0.000755404
Bifidobacteriaceae	0.000733187
Rhizobiaceae	0.000733187
Peptostreptococcaceae	0.000644316
Nocardioidaceae	0.00059988
Mycoplasmataceae	0.00059988
Caulobacteraceae	0.000577662
Lactobacillaceae	0.000555444
Brevibacteriaceae	0.000511009
Dermabacteraceae	0.000511009
Nocardiaceae	0.000511009
Sphingobacteriaceae	0.000511009
Ruminococcaceae	0.000444356
Rubrobacteraceae	0.000422138
Methylobacteriaceae	0.000422138
Oxalobacteraceae	0.00039992
Halomonadaceae	0.00039992
Deinococcaceae	0.000355484
Lachnospiraceae	0.000355484
Erysipelotrichaceae	0.000311049
Microbacteriaceae	0.000266613
Geodermatophilaceae	0.000244396
Burkholderiales_incertae_sedis	0.000244396
Legionellaceae	0.000244396
Salinisphaeraceae	0.000244396
Coriobacteriaceae	0.000222178
Paenibacillaceae	0.000222178
Carnobacteriaceae	0.000222178
Aeromonadaceae	0.000222178
Planctomycetaceae	0.00019996
Hyphomicrobiaceae	0.00019996
Methylophilaceae	0.00019996
Streptomycetaceae	0.000177742
Phyllobacteriaceae	0.000177742
Rhodospirillaceae	0.000177742
Patulibacteraceae	0.000155524
Thermaceae	0.000155524
Cellulomonadaceae	0.000133307
Pseudonocardiaceae	0.000133307
Brucellaceae	0.000133307
Dietziaceae	0.000111089
Beijerinckiaceae	0.000111089
Rhodocyclaceae	0.000111089

Holophagaceae	8.88711E-05
Cyclobacteriaceae	8.88711E-05
Mycobacteriaceae	6.66533E-05
Nakamurellaceae	6.66533E-05
Bacteroidaceae	6.66533E-05
Eubacteriaceae	6.66533E-05
Bdellovibrionaceae	6.66533E-05
Iamiaceae	4.44356E-05
Sphaerobacteraceae	4.44356E-05
Listeriaceae	4.44356E-05
Incertae Sedis XIV	4.44356E-05
Nitrospiraceae	4.44356E-05
Bartonellaceae	4.44356E-05
Alcaligenaceae	4.44356E-05
Vibrionaceae	4.44356E-05
Dermacoccaceae	2.22178E-05
Synergistaceae	2.22178E-05

II.23. Sequence genomic targets

We developed a new bioinformatics pipeline for identifying novel genomic targets for TaqMan PCR assays for detection and quantification of major wound pathogens (**Figure 9**)

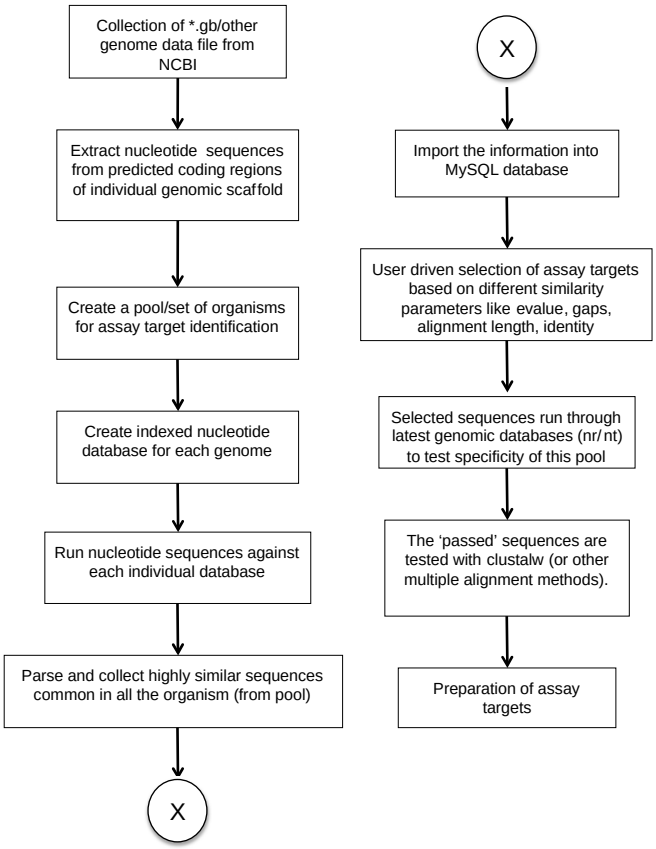

Figure 9. Assay target identification flow-chart

II.24. Develop qPCR assays for top pathogens & validate real time PCR assays for bacterial pathogens.

Originally we set out to develop qPCR assays for the top 40 wound pathogens, but upon investigating the role of *E. coli* in wound infection and sepsis, we found that detection of virulence factors was also critical to evaluating potential risk. Therefore, we redirected our real-time PCR assay design efforts to creating assays for each of the major *E. coli* extra-intestinal virulence factors. (note: we are continuing our effort for developing assays for the top 40 pathogens under a separate award).

ExPEC is a major wound pathogen and responsible for approximately 40,000 sepsis deaths in the U.S. each year. In order to effectively detect Extraintestinal pathogenic *Escherichia coli* (ExPEC) in wound, stool and blood specimens, multiple real-time PCR assays were developed. These assays targeted the six ExPEC hallmark virulence factor (VF) genes and 39 other important virulence genes. The hallmark VF genes were identified by Johnson *et. al.* in 2003 as *papA* and/or *papC*, *afa/dra*, *sfa/foc*, *iutA*, and *kpsMII*; presence of two or more of these genes would classify the strain as ExPEC. The additional 39 VF genes are categorized as adhesins, toxins, siderophores, protectins, as well as eight miscellaneous genes (**Table 5**).

The real-time assay design was completed by compiling publicly available VF gene sequences found in the Enteropathogen Resource Integration Center (ERIC) and NCBI's Genbank, in-house Sanger sequencing was also used. These sequences were used to generate a multiple sequence alignment file. Using the alignment file, conserved regions were identified in each of the VF genes for primer and probe design. Multiple assays (one, two or three per gene) were designed in order to increase levels of sensitivity and reliability. Assay redundancy also allows for unknown mutations, such as single nucleotide polymorphisms (SNPs), to be present or occur in the future under a portion of one assay. In this case, this assay's function could be hindered; however, the remaining primer and probe sets would be unaffected, allowing detection to continue. These redundant detection assays were tested in silico using NCBI BLAST to initially determine primer and probe specificity. Next, cloned plasmids were generated for use during preliminary validation. These cloned standards were quantified, normalized, and sequence-verified. Serial dilution curves of each clone standard were run to test the efficiency of the real-time PCR assays. During these initial runs, the no-template controls were also assessed to determine whether the assay amplified any background or low-level contamination. Genomic DNAs of previously characterized *E. coli* strains were run to determine sensitivity and specificity for the assays.

The results for the initial validation of the 108 assays indicate good utility for detection of the virulence factors (ExPEC assay evaluation table). The adhesin gene assays with 100% sensitivity and specificity based on the characterized set of control strains are all *papA, papC, sfa, focG, afa, iha, clpG, gafD, F17a, fimH* assays, as well as, the papEF1, papEF2, papF, papGI-2, papGIII-1, sfaS1, and sfaS2 assay. A few of the adhesin assays had different results from the former characterization. The *papE* assay was 100% sensitive but only 85.7% specific. The papGIII-2 assay was 100% sensitive but scored low on specificity, finding only seven out of 15 expected positives (46.6%). Both *hra* assays were found to be only 66.6% specific but 100% sensitive. The *sfaS3* assay failed at both the clone standard and genomic DNA panel validation; this is most likely due to an issue in the assay's design. The *afaE8* assay was unsuccessful due to the unavailability of a clone standard; the *afaE8* gene is highly similar to the *bmaE* gene and it appears the attempted cloning strains only picked up *bmaE*. It is possible that these strains are actually lacking the *afaE8* gene. All the toxin genes had 100% sensitivity and specificity; except of all the pic assays were only 87.5% specific and the *tsh* assays were only positive for one of the two expected positive strains, this equated to the *tsh* assays having a 50% sensitivity. Siderophore genes *iutA* and *ireA* were found to be 100% sensitive and specific. While the siderophore gene *fyuA* assays were positive for 14 of 16 expected positives indicating a sensitivity of 87.5% and specificity of two positive strains out of three expected positives (66.6%). The *iroN* assays were both 90.9% sensitive, positive for ten out of eleven expected positive strains; and 87.5% specific, negative for seven of eight expected negative strains. The protectin assays were all 100% sensitive and specific based on the characterized control strains. For the miscellaneous assays, all *ibeA*, *H7-fliC*, *usp*, *PAI*, *uidA*, *clbB* and *clbN* assays were perfectly sensitive and specific according to the prior characterization of the control strains. The only miscellaneous gene with less than perfect sensitivity is *ompT*, the three assays were 93.75% sensitive.

Table 5. ExPEC assay performance.

Category	Gene(s)	Assay	Efficiency	R^2	Sensitivity	Specificity
Adhesins						

pap					
papA					
	papA1	113.28	0.995	14/14 100%	5/5 100%
	papA2	112.23	0.995	14/14 100%	5/5 100%
papC					
	papC1	116.56	0.998	13/13 100%	5/5 100%
	papC2	109.18	0.997	13/13 100%	5/5 100%
	papC3	110.68	0.998	13/13 100%	5/5 100%
papEF					
	papEF1	103.98	0.995	12/12 100%	7/7 100%
	papEF2	108.68	0.996	12/12 100%	7/7 100%
	papE	108.20	0.997	12/12 100%	6/7 85.7%
	papF	103.54	0.992	12/12 100%	7/7 100%
papG allele I'					
	papGI-2	111.19	0.994	1/1 100%	19/19 100%
papG allele III					
	papGIII-1	100.92	0.997	5/5 100%	15/15 100%
	papGIII-2	111.71	0.996	5/5 100%	7/15 46.6%
sfa/foc					
	sfa/foc1	118.26	0.996	8/8 100%	11/11 100%
	sfa/foc2	113.81	0.995	8/8 100%	11/11 100%
	sfa/foc3	117.69	0.996	8/8 100%	11/11 100%
sfaS					
	sfaS1	104.89	0.991	3/3 100%	16/16 100%
	sfaS2	103.54	0.989	3/3 100%	16/16 100%
	sfaS3	N/A	N/A	N/A	N/A
focG					
	focG1	103.54	0.996	5/5 100%	14/14 100%
	focG2	104.89	0.997	5/5 100%	14/14 100%
	focG3	105.82	0.996	5/5 100%	14/14 100%
afa/dra					
	afa1	106.76	0.997	1/1 100%	17/17 100%
	afa2	103.54	0.992	1/1 100%	17/17 100%
	afa3	110.68	0.987	1/1 100%	17/17 100%
afaE8					
	afaE8	N/A	N/A	N/A	N/A
iha					
	iha1	118.26	0.999	6/6 100%	13/13 100%
	iha2	116.56	0.999	6/6 100%	13/13 100%
	iha3	113.81	0.999	6/6 100%	13/13 100%
bmaE					
	bmaE	112.75	0.995	1/1 100%	17/17 100%
gafD					
	gafD-F17-1	119.43	0.997	3/3 100%	16/16 100%
	gafD-F17-2	112.75	0.997	3/3 100%	16/16 100%

	f17				
	F17a	N/A	N/A	1/1 100%	17/17 100%
	clpG				
	clpG1	118.26	0.997	1/1 100%	17/17 100%
	clpG2	117.69	0.997	1/1 100%	17/17 100%
	clpG3	116.56	0.999	1/1 100%	17/17 100%
	fimH				
	fimH1	105.82	0.992	19/19 100%	1/1 100%
	fimH2	104.44	0.991	19/19 100%	1/1 100%
	fimH3	102.65	0.99	19/19 100%	1/1 100%
	hra				
	hra1	121.83	0.998	7/7 100%	9/11 81.8%
	hra2	120.62	0.997	7/7 100%	9/11 81.8%
Toxins					
	hlyD				
	hlyD1	117.69	0.998	9/9 100%	9/9 100%
	hlyD2	114.35	0.997	9/9 100%	9/9 100%
	hlyD3	111.71	0.996	9/9 100%	9/9 100%
	hlyF				
	hlyF1	103.31	0.991	2/2 100%	16/16 100%
	hlyF2	108.68	0.996	2/2 100%	16/16 100%
	cnf1				
	cnf1-1	113.28	0.997	6/6 100%	13/13 100%
	cnf1-2	113.28	0.998	6/6 100%	13/13 100%
	cnf1-3	111.19	0.994	6/6 100%	13/13 100%
	cdtB				
	cdtB-A	116.56	0.998	2/2 100%	16/16 100%
	cdtB-B	N/A	N/A		
	sat				
	sat1	111.71	0.996	5/5 100%	13/13 100%
	sat2	111.71	0.998	5/5 100%	13/13 100%
	astA				
	astA	122.44	0.998	1/1 100%	17/17 100%
	pic				
	pic1	116.56	0.999	5/5 100%	12/13 92.3%
	pic2	111.19	0.999	5/5 100%	12/13 92.3%
	pic3	117.69	0.999	5/5 100%	12/13 92.3%
	tsh				
	tsh1	118.26	0.998	1/2 50%	8/8 100%
	tsh2	117.12	0.999	1/2 50%	8/8 100%
	vat				
	vat1	120.02	0.999	10/10 100%	8/8 100%
	vat2	119.43	0.999	10/10 100%	8/8 100%
Siderophores					
	fyuA				
	fyuA1	116.00	0.999	15/17 88.2%	2/2 100%

	fyuA2	117.69	0.999	15/17 88.2%	2/2 100%
iutA					
	iutA1	111.71	0.999	9/9 100%	10/10 100%
	iutA2	114.89	0.999	9/9 100%	10/10 100%
	iutA3	116.00	0.999	9/9 100%	10/10 100%
iroN					
	iroN1	105.35	0.994	10/10 100%	8/9 88.8%
	iroN2	106.76	0.998	10/10 100%	8/9 88.8%
ireA					
	ireA1	123.07	0.998	7/7 100%	12/12 100%
	ireA2	119.43	0.999	7/7 100%	12/12 100%
	ireA3	117.69	0.999	7/7 100%	12/12 100%
Protectins					
kpsM II					
	kpsMII1	116.56	0.999	10/10 100%	9/9 100%
	kpsMII2	118.26	0.999	10/10 100%	9/9 100%
kpsMT III					
	kpsMIII1	118.26	0.994	2/2 100%	18/18 100%
	kpsMIII2	118.84	0.994	2/2 100%	18/18 100%
	kpsMIII3	120.62	0.447	2/2 100%	18/18 100%
K15					
	K15-1	116.00	0.999	1/1 100%	17/17 100%
	K15-2	116.00	0.999	1/1 100%	17/17 100%
rfc					
	rfc1	119.43	0.998	3/3 100%	16/16 100%
	rfc2	114.89	0.999	3/3 100%	16/16 100%
	rfc3	118.84	0.998	3/3 100%	16/16 100%
cvaC					
	cvaC1	117.12	0.999	2/2 100%	17/17 100%
	cvaC2	116.56	0.999	2/2 100%	17/17 100%
iss					
	iss1	113.28	0.999	2/2 100%	17/17 100%
	iss2	113.28	0.999	1/1 100%	17/17 100%
	iss3	109.67	0.999	1/1 100%	17/17 100%
traT					
	traT1	111.19	0.999	13/13 100%	6/6 100%
	traT2	107.71	0.999	13/13 100%	6/6 100%
	traT3	104.89	0.999	13/13 100%	6/6 100%
Misc.					
ompT					
	ompT1	114.89	0.999	18/19 94.7%	1/1 100%
	ompT2	112.23	0.999	18/19 94.7%	1/1 100%
	ompT3	116.00	0.999	18/19 94.7%	1/1 100%
ibeA					
	ibeA1	116.00	0.997	1/1 100%	18/18 100%

	ibeA2	112.23	0.998	1/1 100%	18/18 100%
	ibeA3	113.81	0.997	1/1 100%	18/18 100%
H7 fliC					
	H7-fliC1	110.17	0.999	1/1 100%	18/18 100%
	H7-fliC2	108.20	0.999	1/1 100%	18/18 100%
	H7-fliC3	109.18	0.998	1/1 100%	18/18 100%
usp					
	usp1	108.68	0.998	10/10 100%	8/8 100%
	usp2	112.23	0.998	10/10 100%	8/8 100%
	usp3	111.19	0.998	10/10 100%	8/8 100%
PAI					
	PAI1	111.19	0.999	11/11 100%	8/8 100%
	PAI2	109.67	0.999	11/11 100%	8/8 100%
	PAI3	111.19	0.999	11/11 100%	8/8 100%
uidA					
	uidA	111.71	0.998	11/11 100%	0/0 100%
clbB					
	clbB1	118.26	0.997	8/8 100%	5/5 100%
	clbB2	118.26	0.997	8/8 100%	5/5 100%
clbN					
	clbN1	116.00	0.998	8/8 100%	5/5 100%
	clbN2	118.26	0.996	8/8 100%	5/5 100%

Further investigation, involving sequencing of the gene and surrounding area of any VF gene assays with discrepancies between current real-time PCR detection and prior characterization is desired to determine accurate gene presence and assay performance. Also, clone standards will be generated for the genes that are missing them.

Future validation of the 108 assays will include a large panel of diverse, well-characterized *E. coli* strains, as well as a broad panel of DNA from *Enterobacteriaceae,* and a diverse panel of all bacteria to further check specificity. Once the assays are further validated and characterized they can be utilized simultaneously in a high-density platform. This high-density array of assays can then be used to efficiently detect and characterize *E. coli* strains in clinical and environmental specimens.

II.25. Methods Development

The bacterial loads in the burn wounds tested to date are very low, which makes the microbial community analysis vulnerable to distortion by exogenous bacterial DNA introduced in commercial enzymes and DNA isolations kits.

We tested several different methods for nucleic acid isolation that minimized contamination with exogenous nucleic acids and PCR inhibitors. We found that poor performance and contamination were prevalent among commercially available kits (including MoBio PowerSoil, the kit recommended by the NIH Human Microbiome Project). After months of trials, we finally settled on a new procedure: physical disruption using the Barocycler NEP3229 (Pressure BioSciences, Inc) followed by DNA, RNA and protein purification using the Qiagen AllPrep kit (Qiagen). Since deciding on the Barocycler procedure, we have also tested a number of conditions to optimize DNA, RNA and protein recovery including: temperature; maximum pressure; cycle number; and cylcle length.

III. KEY RESEARCH ACCOMPLISHMENTS

- Developed and applied a rapid, qPCR-based method for assessing bacterial load in wounds
- Developed and applied a novel, culture-independent pyrosequencing approach to characterize bacterial communities in wounds
- Pioneered an ecological-based statistical approach for analyzing microbial communities in a clinical context
- Revealed association between antibiotic therapy and increased *Pseudomonas* colonization in chronic wounds
- Revealed association between diabetes and *Streptococcus* colonization in chronic wounds
- Characterized bacterial phylotypes among chronic wounds
- Characterized spatial variation in chronic wounds
- Engineered qPCR assays for the rapid detection of clinical pathogens
- Developed a secure web-based sample tracking and analysis system
- Developed over 100 TaqMan real time PCR assays for all of the major extraintestinal pathogen *E. coli* (ExPEC) virulence factors
- Developed a high yield, low contamination protocol for isolating bacterial DNA from burn wound samples
- Engineered a new bioinformatics pipeline for identifying novel genomic targets for TaqMan PCR assays for detection and quantification of major wound pathogens
- Enrolled 71 burn wound patients into a prospective study of burn wound colonization
- Collected and banked 721 wound samples (curettes and swabs) from our prospective burn patient cohort

IV. REPORTABLE OUTCOMES

Publications and Presentations

- **Manuscripts:**
    - Price LB, Liu CM, Frankel YM, Melendez JH, Aziz M, Buchhagen J, Contente-Cuomo T, Engelthaler DM, Keim PS, Ravel J, Lazarus GS, Zenilman JM. Macroscale spatial variation in chronic wound microbiota: a cross-sectional study. Wound Repair Regen. 2011 Jan;19(1):80-8. doi: 10.1111/j.1524-475X.2010.00628.x. Epub 2010 Oct 13. PubMed PMID: 20946140; PubMed Central PMCID: PMC3022109.

    - Frankel YM, Melendez JH, Wang NY, Price LB, Zenilman JM, Lazarus GS. Defining wound microbial flora: molecular microbiology opening new horizons. Arch Dermatol. 2009 Oct;145(10):1193-5. PubMed PMID: 19841413.

    - Price LB, Liu CM, Melendez JH, Frankel YM, Engelthaler D, Aziz M, Bowers J, Rattray R, Ravel J, Kingsley C, Keim PS, Lazarus GS, Zenilman JM. Community analysis of chronic wound bacteria using 16S rRNA gene-based pyrosequencing: impact of diabetes and antibiotics on chronic wound microbiota. PLoS One. 2009 Jul 31;4(7):e6462. PubMed PMID: 19649281; PubMed Central PMCID: PMC2714066.

    - Cindy M Liu, Maliha Aziz, Sergey Kachur, Po-Ren Hsueh, Yu-Tsung Huang, Paul Keim and Lance B Price. BactQuant: An enhanced broad-coverage bacterial quantitative real-time PCR assay. BMC Microbiology. Under Review

- **Presentation:**
    - Presented results at the 48th Annual ICAAC/IDSA 46th Annual Meeting
    - "Data Tools and Computational Challenges," The Tramatic Wound Microbiome Meeting, May 9-10, 2011, at the Walter Reed Army Institute of Research (WRAIR), in Forest Glen, Maryland.

V. CONCLUSION

We developed a suite of advanced molecular tools and techniques to characterize wound microbiota in a culture-independent and minimally-biased fashion. We demonstrated the utility of our assays and methods by applying them to acute burns and chronic wounds. The tools, techniques, and sample repositories that we have generated under this award will be invaluable resources to wound care physicians and researchers into the future.